JOURNAL OF MAGNETIC RESONANCE 89, 60–93 (1990)

Theory of Two-Dimensional ESR with Nuclear Modulation*

DAN GAMLIEL AND JACK H. FREED

Baker Laboratory of Chemistry, Cornell University, Ithaca, New York 14853-1301

Received November 7, 1989; revision received February 5, 1990

A formalism for computing 2D ESR lineshapes with nuclear modulation is developed in a form which is useful for planning phase cycles for particular purposes. A simple method of processing spectra, utilizing quadrature detection, is shown to enhance the selectivity of the phase cycling techniques. Computed ESR-COSY, ESR-SECSY, and 2D ELDOR lineshapes are presented for several kinds of polycrystalline and single-crystal samples which exhibit nuclear modulation, due to one or several nuclei. The two-dimensional methods are found to give more detailed structural information than the corresponding ESEEM spectra. New phase cycles are found to eliminate completely all transverse and axial peaks in 2D ELDOR and in ESR-COSY, and at the same time eliminate all artifacts arising from incomplete image rejection. Other phase cycles are presented for selecting in those experiments only axial peaks, for measuring T_1. It is also shown how selective phase cycles may help to distinguish between coherent and exchange cross peaks. In the special case of nitroxides in typical Zeeman fields, there are no significant nuclear modulation effects from the ^{14}N nuclear spin interaction, but those from the protons (or deuterons) will, in general, be significant.

It has been known for a long time that hyperfine interactions can be investigated via the so-called "nuclear modulation" which they induce in electron spin-echo envelope lineshapes (*1–7*). The magnitude of this modulation is appreciable if the hyperfine coupling of nuclei to the unpaired electron is similar in magnitude to the Zeeman frequency of these nuclei. The details of the modulation depend on the nuclei involved (*8, 9*) and their arrangement relative to the electron (*10*). This has been used to investigate structural properties, such as the environment of ions and radicals in single crystals and in disordered systems (*7, 11*).

Traditionally such investigations have been carried out mainly with the spin-echo experiment or the stimulated spin-echo experiment (*2, 7*). In a recent work, phase cycling was used to eliminate certain artifacts from the stimulated echo experiment (*12*). Moreover, 2D FT versions of the stimulated echo sequence (*13*) and of more general pulse sequences (*14*) have been developed, which yield more accurate and more general structural information than the one-dimensional experiments. These experiments, however, were limited to a narrow bandwidth. At the same time new pulsed ESR techniques which are capable of broadband coverage appropriate for nitroxides have been developed and have consequently been used for various applications (*15–23*). The purpose of the present work is to explore the potential of these

* Supported by NSF Grant CHE8703014 and NIH Grant GM25862.

0022-2364/90 $3.00

techniques of two-dimensional ESR (2D ESR) for systems which exhibit nuclear modulation.

We start with general formulas for the lineshapes in sequences of two, three, and four pulses, including phenomenological relaxation terms. The expressions clearly distinguish different types of contributions to the spectrum. The effect of various kinds of stochastic processes is then briefly considered. It is shown directly that for N-site exchange it is impossible to separate the coherent from incoherent cross peaks by means of phase cycling, and then the same conclusion is reached for other kinds of exchange as well.

It is then shown how to design phase cycles which cancel particular parts of the spectrum for the ESR-COSY and ESR-SECSY pulse sequences. In particular we show how to simultaneously eliminate axial peaks and effects of incomplete image rejection, in order to focus on the interesting parts of the spectrum, which contain important information on the nuclear modulation. We also show how to retain only axial peaks for measuring T_1. It is shown that quadrature detection enables one to enhance the selectivity of phase cycling by a simple method of spectral processing. Both the various phase cycles and the new way of spectral processing can be applied, of course, also to heteronuclear NMR. Several computed lineshapes for ESR-COSY and ESR-SECSY are then presented, demonstrating the kinds of information that can be obtained with these techniques in systems with significant nuclear modulation. It is evident, both from the single crystal spectra and from the polycrystalline spectra, that when nuclear modulation gives rise to spectra which contain nontrivial information on molecular structure, the 2D techniques give more detailed information on the structure of the sample.

We then treat in a similar way the 2D ELDOR sequence and some of its variants, including the addition of a refocusing π pulse, on systems with nuclear modulation, and simulated lineshapes are presented. The results show the potential of the method for investigating structure, and also demonstrate the potential of some new phase cycles together with the new way of data processing. In particular it is shown how simple data processing after the collection of the phase cycled signals can be used to facilitate the distinction between coherent cross peaks, resulting from nuclear modulation, and exchange cross peaks. A short summary and a discussion are finally given.

GENERAL FORMALISM

Calculation for the rigid limit. In order to calculate the ESR signal one has to follow the evolution of the density matrix ρ, governed by the equation (in angular frequency units) (*23–25*):

$$\frac{d}{dt}\rho = -i[\hat{\mathscr{H}}(t), \rho(t)] - \Gamma(\rho(t) - \rho_0(t)). \qquad [1]$$

The difference between the time-dependent density matrix and the equilibrium density matrix ρ_0 is denoted as $\chi(t) \equiv \rho(t) - \rho_0$, $\hat{\mathscr{H}}(t)$ is the spin Hamiltonian, and Γ is a relaxation superoperator.

The relevant Hamiltonian between pulses is the internal Hamiltonian $\hat{\mathscr{H}}_{\text{int}}$. In the present calculations we assume for convenience that the anisotropic part of the g tensor is axially symmetric. Therefore $\hat{\mathscr{H}}_{\text{int}}$ is, in the rotating frame,

$$\hat{\mathscr{H}}_{\text{int}} = \hat{\mathscr{H}}_0 + \hat{\mathscr{H}}_1 \qquad [2]$$

where, in angular frequency units,

$$\hat{\mathscr{H}}_0 = \bar{g}\frac{\beta_e H_0}{\hbar} S_z - \sum_i \omega_{ni} I_{zi} - \gamma_e \sum_i \bar{a}_i S_z I_{zi} \qquad [3]$$

includes the Zeeman terms and the isotropic hyperfine couplings, and

$$\hat{\mathscr{H}}_1 = F\mathscr{D}^2_{0,0}(\Omega) S_z - \gamma_e \sum_i D_i \Big\{ \mathscr{D}^2_{0,0}(\Omega_i) S_z I_{zi} - \sqrt{\frac{3}{8}} (\mathscr{D}^2_{0,1}(\Omega_i) S_z I_{+i} - \mathscr{D}^2_{0,-1}(\Omega_i) S_z I_{-i}) \Big\} \qquad [4]$$

includes the anisotropic parts of the g and hyperfine tensors. In these equations $\bar{g}$ is the isotropic part of the g tensor, ω_{ni} is the nuclear Larmor frequency for nucleus i, Ω denotes the Euler angles which describe the orientation of the g tensor with respect to the static magnetic field, whereas Ω_i denotes the orientations of the electron-nuclear vectors with respect to the magnetic field. The following definitions are used:

$$\bar{a}_i = \frac{1}{3}(A_{\parallel i} + 2A_{\perp i}), \qquad D_i = \frac{2}{3}(A_{\parallel i} - A_{\perp i})$$

$$F = \frac{2}{3}(g_\parallel - g_\perp)\frac{\beta_e H_0}{\hbar}. \qquad [5]$$

For nuclei with $I \geqslant 1$, the internal Hamiltonian includes, in general, also a quadrupole term, given for the ith nucleus by

$$\mathscr{H}_{Qi} = D_{Qi}\mathscr{D}^2_{0,0}(\Omega_i)(I^2_{zi} - \tfrac{1}{3} I_i(I_i + 1)), \qquad [6]$$

where (*26*)

$$D_{Qi} = \frac{3e^2 q Q_i}{4I_i(2I_i - 1)\hbar}. \qquad [7]$$

As is often assumed, the quadrupolar term will be regarded here for convenience as only a small perturbation in the internal Hamiltonian.

For a polycrystalline sample the signal has to be averaged over orientations. If slow rotational diffusion is present, the calculation procedure is more involved (*23, 25, 27, 28*), but most of our considerations in the present work assume the rigid limit.

The microwave pulses are assumed for simplicity to be sufficiently strong, so that the irradiation Hamiltonian satisfies the requirement $\hat{\epsilon} \gg \hat{\mathscr{H}}_{\text{int}} - \bar{g}(\beta_e H_0/\hbar) S_z$. Thus during each pulse the Hamiltonian can be approximated as

$$\hat{\mathscr{H}} \approx \hat{\epsilon} = \omega_1(S_x \cos(\phi) + S_y \sin(\phi)). \qquad [8]$$

Here ϕ is the phase of the pulse, and its tipping angle is $\theta = \omega_1 t_p$, where t_p is the duration of the pulse.

A phenomenological relaxation model is assumed here, with angle-independent T_1 and T_2. Relaxation during pulses is neglected. Free evolution is then described by

$$\frac{d}{dt}\chi(t) = -i[\hat{\mathscr{H}}_{\text{int}}, \chi(t)] - \Gamma\chi(t) \equiv \Gamma'\chi(t), \qquad [9]$$

where, in the basis of $\hat{\mathscr{H}}_{\text{int}}$,

$$\Gamma'_{ij,kl} = \delta_{ik}\delta_{jl}\left(-i\omega_{ij} - \delta_{ij}\frac{1}{T_1} - (1-\delta_{ij})\frac{1}{T_2}\right) \qquad [10]$$

with ω_{ij} the transition frequency. Equation [9] is readily solved by

$$\chi(t_0 + t)_{ij} = e^{\lambda_{ij}t}\chi(t_0)_{ij}, \qquad [11]$$

where $\lambda_{ij} = \Gamma'_{ij,ij}$. During each pulse, the density matrix evolves according to

$$\frac{d}{dt}\rho(t) = -i[\hat{\epsilon}, \rho(t)] \qquad [12]$$

which leads to (*29*)

$$\rho(t_0 + t_p) = e^{-i\phi S_z}e^{-i\theta S_x}e^{i\phi S_z}\rho(t_0)e^{-i\phi S_z}e^{i\theta S_x}e^{i\phi S_z} \qquad [13]$$

using the standard phase convention (*24*).

Equations [11] and [13] can be used for the respective parts of the pulse sequence. The expressions are somewhat simplified by the fact that $e^{i\phi S_z}$ commutes with Γ, even if some relaxation processes are present (*30*), since we neglect nonsecular terms; this will be considered below in greater detail. Perfect spectral coverage is assumed here for simplicity. If the spectrum is not uniformly irradiated (as is often the case) the spectra may be corrected by the method explained by Gorcester and Freed (*19*).

In order to analyze the lineshape by its components one has to separate terms which differ in their dependence on the pulse phases, and work in the basis of the internal Hamiltonian. We can discuss both objectives on the basis of Mims' representation of such operators, which was originally used for cases with nuclear modulation but with zero phases and standard tipping angles of the pulses (*2, 8*).

For one electron with spin $S = \frac{1}{2}$ interacting with one or more nuclei, the relevant Hilbert space is a tensor product of the Hilbert spaces of the electronic spin and the nuclear spins, so the matrix of each operator in the $|S_z I_z\rangle$ basis is composed of four submatrices. Each of the submatrices can be regarded as operating in a reduced Hilbert space, defined just by the nuclear spin functions. An element of a submatrix between states $|k\rangle$, $|l\rangle$ of the full Hilbert space can thus be regarded as an element between the corresponding states $|k'\rangle$, $|l'\rangle$ of the reduced Hilbert space. If the free Hamiltonian $\hat{\mathscr{H}}_{\text{int}}$ is diagonalized by

$$\begin{pmatrix} \mathbf{T}_\alpha^\dagger & 0 \\ 0 & \mathbf{T}_\beta^\dagger \end{pmatrix}\begin{pmatrix} \hat{\mathbf{H}}_\alpha & 0 \\ 0 & \hat{\mathbf{H}}_\beta \end{pmatrix}\begin{pmatrix} \mathbf{T}_\alpha & 0 \\ 0 & \mathbf{T}_\beta \end{pmatrix} = \begin{pmatrix} \mathbf{E}_\alpha & 0 \\ 0 & \mathbf{E}_\beta \end{pmatrix} \qquad [14]$$

(where α and β refer to the $S_z = \frac{1}{2}$ and $-\frac{1}{2}$ subspaces, respectively), then we define $\mathbf{M} \equiv \mathbf{T}_\alpha^\dagger\mathbf{T}_\beta$. Choosing an initial condition of $\rho_0 \propto S_z$, which corresponds to the high-temperature approximation for equilibrium, the ESR signal of a two-pulse sequence, described schematically as (θ_1, ϕ_1)—τ_1—(θ_2, ϕ_2)—τ_2, depends upon

$$\langle S_x + iS_y \rangle^{(2)} = \alpha_1^{(2)} a_1^{(2)} + \alpha_2^{(2)} a_2^{(2)} + \alpha_3^{(2)} a_3^{(2)} + \beta_1^{(2)} b_1^{(2)}. \qquad [15]$$

The premultiplying factors in this sum are equal to

$$\text{(a)}\ \alpha_1^{(2)} = -\frac{i}{4} e^{i\phi_1} \sin(\theta_1)(1 + \cos(\theta_2))$$

$$\text{(b)}\ \alpha_2^{(2)} = \frac{i}{2} e^{i\phi_2} (1 - \cos(\theta_1)) \sin(\theta_2)$$

$$\text{(c)}\ \alpha_3^{(2)} = \frac{i}{4} e^{i(2\phi_2 - \phi_1)} \sin(\theta_1)(1 - \cos(\theta_2))$$

$$\text{(d)}\ \beta_1^{(2)} = -\frac{i}{2} e^{i\phi_2} \sin(\theta_2). \qquad [16]$$

In the next section, each of these prefactors will appear in a more general form, appropriate when phase cycling is performed. The time-dependent terms in the signal are

$$\text{(a)}\ a_1^{(2)} = \sum_{ij} e^{\lambda_{ji}\tau_2} e^{\lambda_{ji}\tau_1} |M_{i'j'}|^2$$

$$\text{(b)}\ a_2^{(2)} = e^{-\tau_1/T_1} \sum_{ij} e^{\lambda_{ji}\tau_2} |M_{i'j'}|^2$$

$$\text{(c)}\ a_3^{(2)} = \sum_{ijkl} e^{\lambda_{ji}\tau_2} e^{\lambda_{kl}\tau_1} M_{i'j'} M^{\dagger}_{j'k'} M_{k'l'} M^{\dagger}_{l'i'}$$

$$\text{(d)}\ b_1^{(2)} = \sum_{ij} e^{\lambda_{ji}\tau_2} |M_{i'j'}|^2. \qquad [17]$$

In these summations the indices i, k denote states with $m = S_z = \frac{1}{2}$ and j, l denote states with $m = -\frac{1}{2}$. The primes indicate that $\mathbf{M}$ operates only on the nuclear spins, being defined only in the restricted, d_I-dimensional space of the nuclear spin functions. The basis states chosen for the full space are those which diagonalize $\mathscr{H}_{\text{int}}$, which are products of electronic spin functions and nuclear spin functions. They are assumed to be ordered in the way implied by Eq. [14], so the indices of states in the restricted (nuclear) space, which are indicated by primes, are related to the indices in the full Hilbert space by

$$i' = i, \qquad k' = k, \qquad j' = j - d_I, \qquad l' = l - d_I, \qquad [18]$$

where d_I is the dimension of the restricted Hilbert space, which is $2I + 1$ for a single nucleus. The time intervals τ_1, τ_2 are not necessarily identical with the two independent time variables in the experiment, which are denoted as t_1, t_2. For example, in ESR-COSY $\tau_1 = t_1$ and $\tau_2 = t_2$ but in ESR-SECSY $\tau_1 = t_1$ and $\tau_2 = t_1 + t_2$.

It was shown by Mims that when several nuclei interact with the electron, the signal is a product of the individual signals that would be obtained if each of the nuclei were the only nucleus to interact with the electron (*2*). This is because $\mathbf{M}$ is a direct product of appropriate matrices. In our case, this rule applies separately to each of the summations in Eq. [17], and not to the whole signal such as in Eq. [15] (as noted in a more restricted context by Dikanov *et al.* (*8*)). Thus, each of these summations has to be

TABLE 1

Coherence Orders in a Two-Pulse Sequence

$\Delta m(\tau_1)$		
−1	0	1
A_1	A_2, B_1	A_3

calculated for the system electron–nucleus for each of the nuclei, and then, for example, the product

$$a_1^{(2)} = \prod_j a_{1,j}^{(2)}, \qquad [19]$$

with the index j running over the nuclei, replaces the simple term for $a_1^{(2)}$, and the same is done for the other terms. In this product, the term $a_{1,j}^{(2)}$ contains the information about the orientation of the electron-nucleus j vector with respect to the molecular coordinate system. The form of Eq. [15] is also convenient for a second reason. If a phase cycle is applied, we do not have to calculate the whole signal repeatedly—only the prefactors have to be summed over, as will be done in the following sections.

Table 1 characterizes the individual summations in Eq. [17] by the quantum order of the transitions which each of them involves in the first time period. Since the measured signal involves transitions with $m_j - m_i = -1$, the Fourier transformed transverse interference term $A_1 \equiv \alpha_1 a_1$ includes in ESR-COSY only autopeaks on the "positive diagonal" ($\omega_1 = \omega_2$). On the other hand, the "echo term" $A_3 \equiv \alpha_3 a_3$ includes peaks on the "negative diagonal" ($\omega_1 = -\omega_2$) as well as an array of cross peaks which is symmetrical around the negative diagonal. Each frequency $\omega_{ji} \equiv -\mathrm{Im}(\lambda_{ji})$ (in the ω_2 domain) has cross peaks with $-\omega_{ik}$ (in ω_1 domain) for all ω_{ik}. The sum of $B_1 \equiv \beta_1 b_1$ and $A_2 \equiv \alpha_1 a_1$ represents longitudinal magnetization which relaxed back from the x–y plane to the z direction during the first time interval, τ_1, and was then rotated by the second pulse into the transverse plane. In the doubly Fourier transformed two-dimensional spectrum determined by

$$\langle S_+ \rangle(\omega_1, \omega_2) = \int_0^\infty dt_1 \int_0^\infty dt_2 e^{-i\omega_1 t_1} e^{-i\omega_2 t_2} \langle S_+ \rangle(t_1, t_2) \qquad [20]$$

these two terms will give rise to axial peaks, on the $\omega_1 = 0$ axis. In a polycrystalline sample, the signal in Eq. [20] has to be averaged over all orientations of a molecule-fixed coordinate system with respect to the laboratory coordinate system, defined by the direction of the static magnetic field and the direction of microwave irradiation.

If the second time interval, τ_2, is not varied independently of τ_1 the directions of the axes and diagonals will of course be changed. For example, in ESR-SECSY, in which $\tau_1 = t_1$ and $\tau_2 = t_1 + t_2$ (t_1 and t_2 are varied independently), the line of the A_1 peaks is rotated to the line $\omega_1 = 2\omega_2$, the line of the axial peaks is rotated to the positive diagonal, and the array of peaks of A_3 is rotated to the $\omega_1 = 0$ axis. This means that the A_3 term is the one responsible for the echo, if we do the echo experiment with $\tau_2 = \tau_1$, and inhomogeneous broadening occurs. The frequencies and line intensities

TABLE 2

Coherence Orders in a Three-Pulse Sequence

	$\Delta m(\tau_1)$		
$\Delta m(\tau_2)$	−1	0	1
−1	A_1	A_2, B_1	A_3
0	A_4	A_5, B_2, C_1	A_6
1	A_7	A_8, B_3	A_9

derived in that case from $a_3^{(2)}$ are the same as in Mims' formulas for the spin-echo modulation (*2*). The frequency doubling along the ω_1 axis results from our definition of t_1, which corresponds to the convention in electron spin-echo experiments. The apparent doubling is avoided if one defines $\tau_1 = t_1/2$, $\tau_2 = t_1/2 + t_2$, as is commonly done in NMR (*24*). Unlike in ESR-COSY, here the off-diagonal peaks for each ω_{ji} (in the ω_2 domain) are with $\omega_{ji} - \omega_{lk}$ (in the ω_1 domain) for all ω_{lk}.

If the sequence consists of three pulses, schematically given as (θ_1, ϕ_1)—τ_1—(θ_2, ϕ_2)—τ_2—(θ_3, ϕ_3)—τ_3, the signal is

$$\langle S_x + iS_y \rangle^{(3)} = \sum_{j=1}^{9} \alpha_j^{(3)} a_j^{(3)} + \sum_{j=1}^{3} \beta_j^{(3)} b_j^{(3)} + \gamma_1^{(3)} c_1^{(3)}. \qquad [21]$$

The prefactors and the time-dependent sums are listed in the Appendix. We present here only the two summations that are important in 2D ELDOR:

$$a_4^{(3)} = \sum_{ijkl} e^{\lambda_{ji}\tau_3}(e^{\lambda_{ji}\tau_2}e^{\lambda_{jk}\tau_1} + e^{\lambda_{ki}\tau_2}e^{\lambda_{li}\tau_1})M_{i'j'}M^{\dagger}_{j'k'}M_{k'l'}M^{\dagger}_{l'i'}$$

$$a_6^{(3)} = \sum_{ijkl} e^{\lambda_{ji}\tau_3}(e^{\lambda_{ji}\tau_2}e^{\lambda_{kl}\tau_1} + e^{\lambda_{ki}\tau_2}e^{\lambda_{kl}\tau_1})M_{i'j'}M^{\dagger}_{j'k'}M_{k'l'}M^{\dagger}_{l'i'} \qquad [22]$$

The transverse terms are, in the present notation, A_1, A_7, A_3, and A_9. It should be noted that, unlike in the absence of nuclear modulation, most of the transverse terms (A_7, A_3, and A_9) include off-diagonal peaks, interfering with those of the "2D ELDOR terms" A_4 and A_6. Only A_1 does not have any cross peaks. The axial$_E$ terms are in the present notation $A_2 + B_1$ and $A_8 + B_3$, while A_5, B_2, and C_1 are the axial$_M$ terms. All these components of the three-pulse ESR lineshape are discussed below in detail for the 2D ELDOR sequence.

As in the two-pulse case, there are two independent time variables, which are Fourier transformed. These are often, but not always, identical with τ_1 and τ_3. The additional time interval in the three-pulse case is regarded as a parameter, but could be utilized in a 3D technique.

As seen previously, if more than one nucleus is present, one has to take the appropriate products for each of the 13 summations $a_j^{(3)}$, $b_j^{(3)}$, $c_j^{(3)}$ separately, while phase cycles involve only the prefactors. Table 2 characterizes each of the components of the signal by the quantum order of the related transitions during the first two time intervals. On Fourier transforming the signal, A_1, A_4, and A_7 create peaks on and symmetrically around the positive diagonal, A_3, A_6, and A_9 generate peaks on and

symmetrically around the negative diagonal, and all other terms generate axial peaks. If one measures just the echo for $\tau_3 = \tau_1$, the term which is observed (in the presence of inhomogeneous broadening) is A_6, which is in this case the same as the expression given by Mims for the stimulated echo experiment (*2*). The axial term $A_8 + B_3$ is the corresponding echo term for $\tau_3 = \tau_2$.

In some cases one may be interested in adding a fourth, refocusing, pulse to avoid dead-time problems. It is therefore important to know how the refocused spectrum is related to the ordinary 2D ELDOR spectrum. The four-pulse lineshape is generally given by the expression

$$\langle S_x + iS_y \rangle^{(4)} = \sum_{ij} (S_x + iS_y)_{ij} e^{\lambda_{ji}\tau_4} e^{-i\phi_4(m_j - m_i)} \sum_{kl} e^{i\phi_4(m_k - m_l)} (V_4^\dagger)_{jk} (V_4)_{li} \rho_{kl}^{(3)}, \quad [23]$$

where $\rho^{(3)}$ is the density matrix just before the fourth pulse and $V_4 \equiv e^{i\theta_4 S_x}$. If the fourth pulse has a tipping angle of π, then the important terms in the lineshape are

$$a_4^{(4)} = \sum_{ijklrs} e^{\lambda_{ji}\tau_4} e^{\lambda_{rs}\tau_3} (e^{\lambda_{rl}\tau_2} e^{\lambda_{rk}\tau_1} + e^{\lambda_{ks}\tau_2} e^{\lambda_{ls}\tau_1}) M_{i'j'} M_{j'r'}^\dagger M_{r'k'} M_{k'l'}^\dagger M_{l's'} M_{s'i'}^\dagger$$

$$a_6^{(4)} = \sum_{ijklrs} e^{\lambda_{ji}\tau_4} e^{\lambda_{rs}\tau_3} (e^{\lambda_{rl}\tau_2} e^{\lambda_{kl}\tau_1} + e^{\lambda_{ks}\tau_2} e^{\lambda_{kl}\tau_1}) M_{i'j'} M_{j'r'}^\dagger M_{r'k'} M_{k'l'}^\dagger M_{l's'} M_{s'i'}^\dagger. \quad [24]$$

In the three-pulse sequence, A_4 included for each frequency ω_{ji} only cross peaks with frequencies ω_{jk} or ω_{li}, i.e., frequencies which had one level in common with it. After the refocusing pulse, cross peaks appear with frequencies ω_{rk} or ω_{ls}, which do not necessarily have any level in common with ω_{ji}. In A_6, on the other hand, a full array of cross peaks existed already after three pulses, so the fourth pulse is not expected to significantly affect the form of this part of the spectrum. This different behavior of the two spectral terms is manifested in simulated results presented below.

Calculation with stochastic processes. So far relaxation has been included only in a phenomenological manner. In practice one is often concerned with nontrivial effects of relaxation processes. In one type of stochastic process the spin probe has N different sites, differing by their spin Hamiltonians (*23, 31–34*), and a random exchange process transfers spins between the different sites (*23, 25*). Another type is rotational diffusion, isotropic or anisotropic, which involves a continuous range of orientations with respect to the magnetic field, which are the "sites" in this case (*23, 25, 27*). In both types of processes, the m value of the electronic spin functions is unaffected by the random exchange or diffusion. In Heisenberg exchange, the total S_z value of the two electrons is unaffected by the process, so the same situation holds (*35, 36*). We shall outline here the way in which the lineshape calculation is modified when stochastic processes are included. In particular we shall show that one cannot separate coherent from incoherent cross peaks without resorting to methods which involve either many repetitions of the basic experiment with random changes in the mixing time or decreasing the resolution (*37*).

In each of these cases, the superoperator Γ' of Eq. [9] may be diagonalized, so that

$$(e^{\Gamma' t})_{ij,kl} = \sum_{mn} \Theta_{ij,mn} e^{\lambda_{mn} t} \Theta^{-1}_{mn,kl}, \quad [25]$$

where $\lambda_{mn} = \Lambda_{mn,mn}$ are the eigenvalues of Γ', and the columns of Θ are the eigenvec-

tors of Γ'. In general, this expansion of the time-dependent exponents implies the appearance of exchange cross peaks. Of particular interest are the A_1 term for ESR-COSY and A_1 for 2D ELDOR, the only terms in the respective spectra which lead just to autopeaks in the absence of exchange.

Consider first the case of N-site jumps. In that case, the equation of motion for the density matrix is (omitting T_1, T_2 terms which could result from other relaxation processes) (*38*)

$$\frac{d}{dt}\rho^{(i)} = i[\rho^{(i)}, \hat{\mathscr{H}}^{(i)}] - \sum_{i,j} \Gamma_{ij}\rho^{(j)}. \tag{26}$$

For the simple case of $N = 2$, the jump matrix is given by (*25*)

$$\Gamma = \frac{1}{\tau}\begin{pmatrix} 1 & -1 \\ -1 & 1 \end{pmatrix}. \tag{27}$$

The relevant Liouville space for N-site exchange is a direct sum of the Liouville spaces of the N individual sites (*39, 40*). Its basis states may be denoted as $|i^{(n)}\rangle\langle j^{(n)}|$, where n is the site index and $|i^{(n)}\rangle$, $|j^{(n)}\rangle$ are basis states of the Hilbert space for site n, assumed to diagonalize the Hamiltonian of that site. It is convenient to order the basis states so that for each (i,j) all n values are scanned before changing (i,j):

$$|i^{(1)}\rangle\langle j^{(1)}|, |i^{(2)}\rangle\langle j^{(2)}|, \ldots, |i^{(N)}\rangle\langle j^{(N)}|, |i'^{(1)}\rangle\langle j'^{(1)}|, \ldots. \tag{28}$$

Since there are $2d_I \times 2d_I$ different Liouville space vectors for each site, the supermatrix Γ now consists of, $2d_I \times 2d_I$ blocks along its diagonal, each block being of dimension $N \times N$.

The ESR signal for such a system is an average over the signal resulting from all N sites. Since the exchange process does not change the electronic m value, $\Gamma'_{ij,kl} \neq 0$ only for $m_i - m_j = m_k - m_l$, and the same condition is required in order to have $\Theta_{ij,kl} \neq 0$ or $\Theta^{-1}_{ij,kl} \neq 0$ (*30*). Using these facts it is easy to show that for a two-pulse sequence:

$$A_1 = -\frac{i}{4}\sin(\theta_1)(1 + \cos(\theta_2)e^{i\phi_1} \sum_{ij} \sum_{mnkpr} e^{\lambda_{ji}^{(n)}\tau_2} e^{\lambda_{ji}^{(m)}\tau_1} \times M^{(k)}_{i'j'} M^{\dagger(r)}_{j'i'} \Theta^{(k,n)}_{ji,ji} \Theta^{-1(n,p)}_{ji,ji} \Theta^{(p,m)}_{ji,ji} \Theta^{-1(m,r)}_{ji,ji}. \tag{29}$$

[For each Θ operator in Eq. [29], the first two subscripts are related to the first superscript, and the last two are related to the second superscript].

For each index pair (ij), the contribution to the summation in a_1 is therefore (omitting for simplicity the i,j subscripts)

$$\sum_{mnkr} e^{\lambda^{(n)}\tau_2} e^{\lambda^{(m)}\tau_1} M^{(k)} M^{\dagger(r)} \Theta^{(k,n)} \Theta^{-1(m,r)} \sum_{p} \Theta^{-1(n,p)} \Theta^{(p,m)} = \sum_{nkr} e^{\lambda^{(n)}\tau_2} e^{\lambda^{(n)}\tau_1} M^{(k)} M^{\dagger(r)} \Theta^{(k,n)} \Theta^{-1(n,r)}. \tag{30}$$

Thus even in the presence of N-site exchange, A_1 has only autopeaks, so that only in the A_3 term, which includes coherent cross peaks, will exchange cross peaks also appear. Phase cycling can at most isolate a term, like A_1 or A_3, which has a distinct

phase factor, but cannot extract a specific part out of such a term. It is therefore impossible to separate coherent from incoherent cross peaks in ESR-COSY on such an exchanging system just by means of phase cycling. The result found here applies also to A_1 of a three-pulse sequence, so that also for 2D ELDOR the desired separation cannot be obtained for N-site exchange. As explained above, this conclusion applies to Heisenberg exchange as well.

For rotational diffusion one has to expand the density matrix and the Hamiltonian in eigenfunctions of the stochastic superoperator Γ, which are Wigner's rotation matrices (*25*). Equation [9] is then transformed to a similar equation for the expansion coefficients, in which Eq. [30] could still be used, provided we truncate the infinite set of equations at some point (*25, 27*). Thus the same conclusion, concerning the absence of exchange cross peaks in A_1, is also valid here.

Although the two types of cross peaks cannot be separated, they can be distinguished by their temperature dependence and field dependence. For sufficiently low temperatures, exchange cross peaks would have very low intensities, so that nuclear modulation would dominate away from the main diagonal. On the other hand, a significant change in the nuclear Zeeman terms, which can be caused by a corresponding change in the static magnetic field, will have a marked effect on the intensity of nuclear modulation. The intensity of exchange cross peaks is practically independent of the external field, as long as the magnitude of the change in electronic Zeeman interaction, which is affected by the jump process, is not the largest part of the internal Hamiltonian.

In addition to these two methods, phase cycling can also be helpful in simplifying the problem of separating coherent effects from exchange effects. As noted in the previous subsection, in the absence of exchange the A_4 spectral term in 2D ELDOR has only some off-diagonal peaks, unlike A_6 which has a full array of off-diagonal peaks. If an exchange process is present, one may follow the same steps which led to Eq. [29] to obtain for A_4:

$$\begin{aligned} A_4 = \frac{i}{8} e^{i(\phi_3 - \phi_2 + \phi_1)} \sin(\theta_1)\sin(\theta_2)\sin(\theta_3) \sum M^{(a)}_{i'j'} \\ \times \Theta^{(a,b)}_{ji,ji} e^{\lambda^{(b)}_{ji}\tau_3} \Theta^{-1(b,c)}_{ji,ji} \{ \Theta^{(c,d)}_{ki,ki} e^{\lambda^{(d)}_{ki}\tau_2} \Theta^{-1(d,r)}_{ki,ki} \Theta^{(r,s)}_{pi,pi} e^{\lambda^{(s)}_{pi}\tau_1} \\ \times \Theta^{-1(s,u)}_{pi,pi} M^{\dagger(c)}_{k'j'} M^{(r)}_{k'p'} M^{\dagger(u)}_{p'i'} + \Theta^{(c,d)}_{jl,jl} e^{\lambda^{(d)}_{jl}\tau_2} \\ \times \Theta^{-1(d,r)}_{jl,jl} \Theta^{(r,s)}_{jq,jq} e^{\lambda^{(s)}_{jq}\tau_1} \Theta^{-1(s,u)}_{jq,jq} M^{\dagger(c)}_{l'i'} M^{(r)}_{q'l'} M^{\dagger(u)}_{j'q'} \}. \end{aligned} \quad [31]$$

Thus $\omega^{(b)}_{ji}$ has exchange cross peaks with $\omega^{(s)}_{pi}$ and $\omega^{(s)}_{jq}$, but not with frequencies which have no index in common with it. Therefore, A_4 not only has a limited array of coherent cross peaks, but also has (at different points in the two-dimensional spectrum) a limited array of incoherent cross peaks. In the same manner, A_6 has not only a full array of coherent cross peaks, but also a full array of exchange cross peaks. This means that if one selects the spectral term A_4, in ways that will be shown here, the spectrum will be simpler than the ordinary 2D ELDOR spectrum, and it will therefore be easier to disentangle the exchange part from the spectrum.

PHASE CYCLING FOR TWO-PULSE SEQUENCES

Theory. The lineshape formulas given above determine the type of peaks that are observed in specific experiments. For example, in the spin-echo experiment, in which $\theta_1 = \pi/2$, $\theta_2 = \pi$, and $\phi_1 = \phi_2 = 0$ the only nonzero prefactor in Eq. [15] is $\alpha_3^{(2)}$, so that only A_3 is observed. Choosing $\tau_2 = \tau_1$ this is reduced to the standard version of the spin-echo spectrum.

We shall now investigate phase-cycling effects, focusing on sequences with: $\theta_1 = \theta_2 = \pi/2$, in which the prefactors of Eq. [16] are

$$\alpha_1 = -\frac{i}{4}e^{i\phi_1}, \qquad \alpha_2 = -\beta_1 = \frac{i}{2}e^{i\phi_2}, \qquad \alpha_3 = \frac{i}{4}e^{i(2\phi_2-\phi_1)} \tag{32}$$

(the "(2)" superscript is dropped from now on). The two axial terms can then be combined to the familiar expression

$$A_2 + B_1 = \alpha_2(a_2 - b_1) = -\frac{i}{2}e^{i\phi_2}(1 - e^{-\tau_1/T_1})\sum e^{\lambda_{ji}\tau_2}|M_{i'j'}|^2. \tag{33}$$

Selection of particular parts of the signal can be achieved in general by applying a phase cycle to the pulses, and possibly also to the receiver (*24, 41*).

If the complex signal is written as $a + ib$, there are four ways of entering it into the "real" and "imaginary" buffers of the register, Reg_R (memory address 1 or 3) and Reg_I (memory address 2 or 4): adding—$\mathrm{Reg}_R = a$, $\mathrm{Reg}_I = b$; subtracting—$\mathrm{Reg}_R = -a$, $\mathrm{Reg}_I = -b$; interchanging real and imaginary parts after changing the sign of b—$\mathrm{Reg}_R = -b$, $\mathrm{Reg}_I = a$; or after changing the sign of a—$\mathrm{Reg}_R = b$, $\mathrm{Reg}_I = -a$. These four operations are equivalent to multiplying the signal by $f_k = e^{i\phi_R^{(k)}}$ where the receiver phase ϕ_R is equal to 0, π, $\pi/2$, or $3\pi/2$ (in this order), and they also correspond, for example, to steps 1, 3, 4, and 2 (in this order) in each of the phase cycles in Tables 3–5. Given a set of factors f_k, a prefactor, which had the form $\alpha = \kappa e^{i(\mu_1\phi_1+\mu_2\phi_2)}$ for a single-pulse sequence, becomes for the phase cycle

$$\alpha = \kappa \sum_k e^{i\phi_R^{(k)}} e^{i(\mu_1\phi_1^{(k)}+\mu_2\phi_2^{(k)})} \equiv \kappa \sum_k f_k e^{i(\mu_1\phi_1^{(k)}+\mu_2\phi_2^{(k)})}. \tag{34}$$

Specifically,

$$\alpha_1 = -\frac{i}{4}\sum_k f_k e^{i\phi_1^{(k)}}, \qquad \alpha_2 = \frac{i}{2}\sum_k f_k e^{i\phi_2^{(k)}}$$

$$\alpha_3 = \frac{i}{4}\sum_k f_k e^{i(2\phi_2^{(k)}-\phi_1^{(k)})}. \tag{35}$$

For our purpose, it is immaterial whether the "receiver factors" f_k are created by cycling the receiver phase or by manipulating the data in the computer. We shall consider here only two simple cycles of these receiver factors, focusing on the various phase cycles of the pulses that are useful with each of them.

In Table 3a the eight-step phase cycle used by Gorcester and Freed for ESR-COSY is listed (*19*). The values of the receiver factors and the "memory addresses" are based on those given for the four-step CYCLOPS by Hoult and Richards (*42*), differ-

TABLE 3

Phase Cycles for ESR-COSY

Phase cycle	Step	Phases		Memory address[a,b]				Eliminates
		ϕ_1	ϕ_2	1	2	3	4	
(a)	1	x	x	1	2			—
	2	y	y	2	−1			(Nonselective)
	3	$-x$	$-x$	−1	−2			
	4	$-y$	$-y$	−2	1			
	5	y	x			−1	−2	
	6	$-x$	y			−2	1	
	7	$-y$	$-x$			1	2	
	8	x	$-y$			2	−1	
(b)	1	x	x	1	2			Axial terms
	2	y	y	2	−1			
	3	$-x$	x	−1	−2			
	4	$-y$	y	−2	1			
	5	y	x			−1	−2	
	6	$-x$	y			−2	1	
	7	$-y$	x			1	2	
	8	x	y			2	−1	
(c)	1	x	x	1	2			Nonaxial terms
	2	y	y	2	−1			
	3	x	$-x$	−1	−2			
	4	y	$-y$	−2	1			

[a] The contents of memory addresses 1 and 2 forms the real and imaginary parts respectively of S', while addresses 3 and 4 give the real and imaginary parts of S''.

[b] In addition to the phase cycling, the signals, S', S'' may be combined using Eq. [39] or Eq. [41] (see text).

ing from those of Gorcester and Freed. The reason is that in the latter work the phase convention was the opposite of the standard one (see Eq. [13] in the present work), and their receiver factors were modified accordingly. The second half of the eight-step sequence is almost a repetition of the first half, except that ϕ_1 is advanced by $\pi/2$ and, in our phase convention, the phases of the receiver factors are inverted. This doubling of the CYCLOPS sequence is useful for additional manipulation of the signal, as will now be explained.

In the special case of no nuclear modulation and no phase cycling, the ESR-COSY signal is (cf. Eqs. [15]–[17])

$$S' = -\frac{1}{2}\sum_{i,j} e^{\lambda_{ji}\tau_2}\mathrm{Im}(e^{\lambda_{ji}\tau_1})\delta_{i'j'} - \frac{i}{2}(1 - e^{-\tau_1/T_1})\sum_{i,j} e^{\lambda_{ji}\delta_2}\delta_{i'j'} \qquad [36]$$

and upon advancing the phase of the first pulse by $\pi/2$, the corresponding signal is

$$S'' = -\frac{1}{2}\sum_{i,j} e^{\lambda_{ji}\tau_2}\mathrm{Re}(e^{\lambda_{ji}\tau_1})\delta_{i'j'} - \frac{i}{2}(1 - e^{-\tau_1/T_1})\sum_{i,j} e^{\lambda_{ji}\tau_2}\delta_{i'j'}. \qquad [37]$$

These expressions are similar to Eqs. [33] and [34] of Ref. (*19*), with a minor correc-

TABLE 4

Eliminating Transverse and Axial Terms in 2D ELDOR

		Phases			Memory address[a,b]			
Phase cycle	Step	ϕ_1	ϕ_2	ϕ_3	1	2	3	4
(a)	1	x	x	x	1	2		
	2	y	y	y	2	−1		
	3	x	x	$-x$	−1	−2		
	4	y	y	$-y$	−2	1		
	5	x	$-x$	$-x$	1	2		
	6	y	$-y$	$-y$	2	−1		
	7	x	$-x$	x	−1	−2		
	8	y	$-y$	y	−2	1		
	9	y	x	x			−1	−2
	10	$-x$	y	y			−2	1
	11	y	x	$-x$			1	2
	12	$-x$	y	$-y$			2	−1
	13	y	$-x$	$-x$			−1	−2
	14	$-x$	$-y$	$-y$			−2	1
	15	y	$-x$	x			1	2
	16	$-x$	$-y$	y			2	−1
(b)	1	x	$-y$	x	1	2		
	2	y	x	y	2	−1		
	3	x	$-y$	$-x$	−1	−2		
	4	y	x	$-y$	−2	1		
	5	$-y$	x	$-x$	1	2		
	6	x	y	$-y$	2	−1		
	7	$-y$	x	x	−1	−2		
	8	x	y	y	−2	1		
	9	y	$-y$	x			−1	−2
	10	$-x$	x	y			−2	1
	11	y	$-y$	$-x$			1	2
	12	$-x$	x	$-y$			2	−1
	13	x	x	$-x$			−1	−2
	14	y	y	$-y$			−2	1
	15	x	x	x			1	2
	16	y	y	y			2	−1

[a] The contents of memory addresses 1 and 2 forms the real and imaginary parts respectively of S', while addresses 3 and 4 give the real and imaginary parts of S''.

[b] In addition to the phase cycling, the signals S', S'' may be combined using Eq. [39] or Eq. [41] (see text).

tion (Re(···), Im(···) should be interchanged in their equations) and with the addition of the axial terms. In terms of the register, the "real" and "imaginary" buffers Reg_R and Reg_I are the real and imaginary parts, respectively, of S' (if the signal is collected in memory addresses 1, 2) or S'' (if the signal is collected in memory addresses 3, 4).

More generally we denote by A_i' the components of S', and by A_i'' the components of S''. With the phase cycle 3a, all three terms (A_1, A_3, and $A_2 + B_1$) are present.

TABLE 5

Selecting Axial$_M$ Terms in 2D ELDOR

Phase cycle	Step	Phases			Address[a]	
		ϕ_1	ϕ_2	ϕ_3	1	2
(a)	1	x	x	x	1	2
	2	y	y	y	2	−1
	3	x	x	$-x$	−1	−2
	4	y	y	$-y$	−2	1
	5	x	$-x$	x	1	2
	6	y	$-y$	y	2	−1
	7	x	$-x$	$-x$	−1	−2
	8	y	$-y$	$-y$	−2	1
(b)	1	x	y	x	1	2
	2	y	$-x$	y	2	−1
	3	x	y	$-x$	−1	−2
	4	y	$-x$	$-y$	−2	1
	5	y	x	x	1	2
	6	$-x$	y	y	2	−1
	7	y	x	$-x$	−1	−2
	8	$-x$	y	$-y$	−2	1

[a] The contents of memory addresses 1 and 2 forms the real and imaginary parts respectively of S'.

Using this phase cycle there is a simple relation between the signals registered in the two sets of memory addresses

$$A''_1 = -iA'_1, \qquad (A''_2 + B''_1) = -(A'_2 + B'_1), \qquad A''_3 = iA'_3. \tag{38}$$

The two parts of phase cycle 3b are related to each other as the two parts of cycle 3a, so Eq. [38] also applies to 3b, although the axial term $A_2 + B_1$ vanishes in this case, and the equation for this term becomes trivial. On the basis of the quadrature combination that was developed in NMR for obtaining pure absorption lineshapes (*43, 44*) Gorcester and Freed suggested forming the combination

$$S_R = \mathrm{Re}(S') + i\,\mathrm{Re}(S') \tag{39}$$

after Fourier transforming t_2 and before Fourier transforming t_1 (*18, 19*). For ESR-COSY, this is equivalent to taking, when all spectral terms are present,

$$S_R = A'_1 + (1 - i)\mathrm{Re}(A'_2 + B'_1) + A'^*_3. \tag{40}$$

This expression remains valid when some terms vanish due to phase cycling, as in the case of phase cycle 3b. Because this combination is done between the two Fourier transformations, the complex conjugation of A_3 changes the sign of the frequencies in the ω_1 domain but not in the ω_2 domain. This has the effect of rotating the peak array of A'_3 from the negative diagonal to the positive diagonal, while A'_1 remains along the positive diagonal, and the axial peaks are not significantly affected. Baseline subtraction is then needed to eliminate axial peaks, and A_1 and A_3 remain unsepa-

rated. They can be separated, however, by combining the signals in one of the two following ways:

$$S_{C+} = S' + iS'' \qquad \text{or} \qquad S_{C-} = S' - iS''. \tag{41}$$

In the present case, this gives

$$S_{C+} = 2A'_1 + (1 - i)(A'_2 + B'_1)$$

and

$$S_{C-} = (1 - i)(A'_2 + B'_1) + 2A'_3. \tag{42}$$

Again, these expressions are also valid when part of the terms vanish due to phase cycling. The axial peaks still have to be eliminated directly by phase cycling, but either A_1 or A_3 is exactly canceled by these combinations. Thus quadrature detection enables one to get greater spectral selectivity. If inhomogeneous broadening is present, the effects of nuclear modulation are maximized in S_{C-} and minimized in S_{C+}. This is because S_{C-} is the "echo term," whereas S_{C+} is the "FID term." Thus collecting both S' and S'' and then calculating S_{C+} and S_{C-} should be very useful when exchange cross peaks are also present. If S_{C-} is used one may get A_3 in the familiar location, along the main diagonal, by taking the complex conjugate of S_{C-} after the Fourier transform on t_2 and before the transform on t_1. This is the actual procedure that we employed in the ESR-COSY and 2D ELDOR (but not ESR-SECSY) computations done with the S_{C-} combination.

We have carried out a systematic computer search for phase cycles which eliminate axial peaks with the same receiver factors as CYCLOPS. A typical cycle which meets these requirements is given in Table 3b. Instead of incrementing the $0, \pi/2$ phases of both pulses by π, only the phase of the first pulse is incremented in this manner. The result is that the axial terms are canceled together with DC offsets which may distort the FIDs. Also, the full effect of CYCLOPS is retained. For ESR-SECSY experiments, the selection of specific parts of the spectrum is done in exactly the same way as for ESR-COSY. If one wants to measure T_1 with ESR-COSY, one needs phase cycles which select just $A_2 + B_1$ by making $\alpha_1 = \alpha_3 = 0$. This can be accomplished using the phase cycle of Table 3c.

Results of simulations. A few examples will now be given in order to demonstrate potential applications of the phase cycling and spectral processing methods to systems which exhibit nuclear modulation. All the lineshapes to be presented are absolute value lineshapes in the two-frequency domain, as in Eq. [20]. For convenience in comparison with experimental results, the calculation was done by FFT of the time-domain spectrum, with 64 values of t_1 and 64 values of t_2 in each case, where the time increments are denoted by Δt_1 and Δt_2 respectively.

Figure 1 shows a typical simulated ESR-COSY rigid limit spectrum of a single crystal, in which a single proton is coupled to the unpaired electron. The Zeeman term corresponds to a magnetic field of 3300 G, and the hyperfine parameters were chosen as $A_\parallel = 6.5$ G and $A_\perp = -3.25$ G, as an example of strong nuclear modulation (*27*). The hyperfine tensor makes an angle of 30° with the magnetic field. Axial peaks were not included in the calculation, which is equivalent either to having infinite T_1

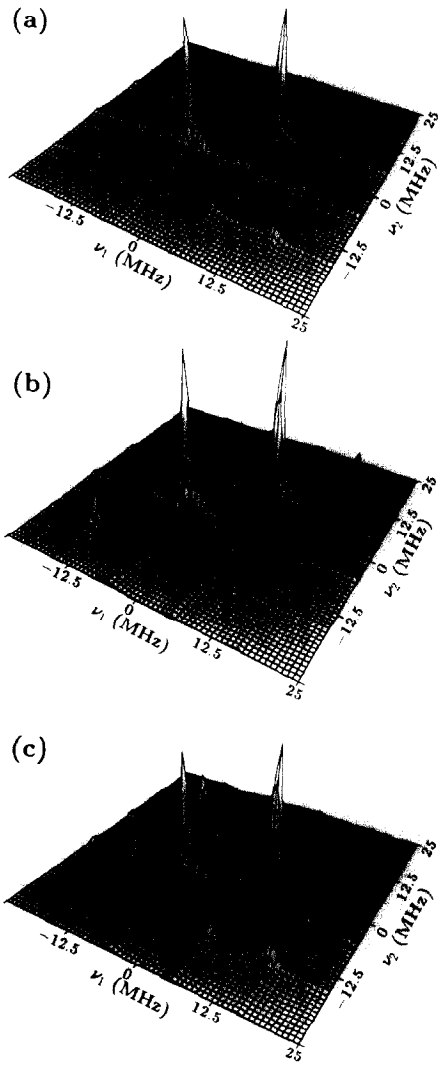

FIG. 1. ESR-COSY spectra of a single crystal, having one proton coupled to the electron, with the hyperfine tensor oriented at 30° with respect to the magnetic field. The spectra are obtained with (a) S_R, (b) S_{C+}, and (c) S_{C-} (see text). The parameters used are $\bar{a} = 0$, $D = 18.2$, $\nu_I = 14.0$, and $F = 0$ (all in MHz). The time parameters are $t_1^{(0)} = 20$, $t_2^{(0)} = 130$, $\Delta t_1 = \Delta t_2 = 20$ and $T_2 = 500$ (all in ns).

and using phase cycle 3a or to having any value of T_1 and using phase cycle 3b. Figure 1a results from the S_R spectral combination, giving $A_1 + A_3$. It contains two strong autopeaks due to "allowed" transitions, which are present even when only secular hyperfine coupling is present, and weaker "nuclear modulation" autopeaks, due to the pseudo-secular part of the hyperfine coupling. In addition to these peaks, which are also observed in CW experiments, the nuclear modulation also gives rise to coherent cross peaks. The location of all these peaks is simply related to the parameters in the Hamiltonian. If one writes the Hamiltonian of Eqs. [2]–[4] for this case as

$$\mathcal{H}_{\text{int}} = CS_z - \omega_n I_z + AS_z I_z + \tfrac{1}{2} BS_z I_+ + \tfrac{1}{2} B^* S_z I_- \qquad [43]$$

the frequencies ω_{ji} in Eq. [17] are

$$\begin{aligned} &C \pm \tfrac{1}{2}(\omega_\alpha - \omega_\beta) \qquad (\text{"allowed" transitions}) \\ &C \pm \tfrac{1}{2}(\omega_\alpha + \omega_\beta) \qquad (\text{"forbidden" transitions}) \end{aligned} \qquad [44a]$$

with the definitions

$$\begin{aligned} \omega_\alpha &= \left(\left(\frac{A}{2} - \omega_n\right)^2 + \left(\frac{B}{2}\right)^2\right)^{1/2} \\ \omega_\beta &= \left(\left(\frac{A}{2} + \omega_n\right)^2 + \left(\frac{B}{2}\right)^2\right)^{1/2}. \end{aligned} \qquad [44b]$$

Figure 1b shows the A_1 component, selected by computing S_{C+}. Figure 1c shows A_3, selected with S_{C-} and "rotated" by complex conjugation, as explained in connection with Eq. [41]. Both components have four lines on the diagonal, but with different relative intensities, corresponding to the different expressions in Eq. [17]. The forbidden peaks are weaker in the A_3 spectrum. On the other hand, cross peaks appear only in A_3 and not in A_1, corresponding to the fact that in Eq. [17] each frequency in the ω_2 domain is connected in A_1 only with the same frequency in ω_1 domain, whereas in A_3 it is connected with all frequencies. This results here in the array of 12 cross peaks. Even in this simple case the inclusion of A_1 in S_R (Fig. 1a) causes interference, complicating the spectrum somewhat. Note also that the S_R spectrum has only half the intensity of the sum of the two spectral components, S_{C+} and S_{C-}, because of the factor of 2 in Eq. [42].

Figure 2 shows the ESR-SECSY simulation for the same case. The S_{C+} spectrum, shown in Fig. 2b, differs from the corresponding ESR-COSY spectrum just in the apparent frequency doubling in the ω_1 domain, resulting from our definition of t_1. The S_{C-} spectrum, on the other hand, is changed by having its diagonal peaks moved to the $\omega_1 = 0$ axis, and its array of cross peaks is "twisted," because in the ω_1 domain its peaks are located at frequency differences, as explained in the previous section. Thus the cross-peak array is now symmetrical with respect to rotation by 180°, rather than with respect to reflection along the diagonal.

For this single-proton case we have from Eqs. [15]–[17] that the S_{C-} ESR-SECSY signal is given by

$$\begin{aligned} S = e^{-(2t_1+t_2)/T_2}\{ & k_+\cos(\omega_- t_2) + k_-\cos(\omega_+ t_2) \\ & + \frac{k}{4}[\cos(\omega_\alpha t_1 + \omega_- t_2) + \cos(\omega_\beta t_1 - \omega_- t_2) - \cos(\omega_-(2t_1 + t_2)) \\ & + \cos(\omega_\alpha t_1 + \omega_+ t_2) + \cos(\omega_\beta t_1 + \omega_+ t_2) - \cos(\omega_+(2t_1 + t_2))]\} \end{aligned}$$

$$\text{where } k = (\omega_n B\, \omega_\alpha \omega_\beta)^2,\ k_\pm = \frac{1}{2}\left(1 - \frac{k}{2} \pm \sqrt{1-k}\right),\ \text{and } \omega_\pm = (\omega_\alpha \pm \omega_\beta)/2. \qquad [45]$$

The S_R spectrum is again half the sum of these two components. The integral of peak intensities over ω_2 for each ω_1 value would give the familiar ESEEM spectrum as a

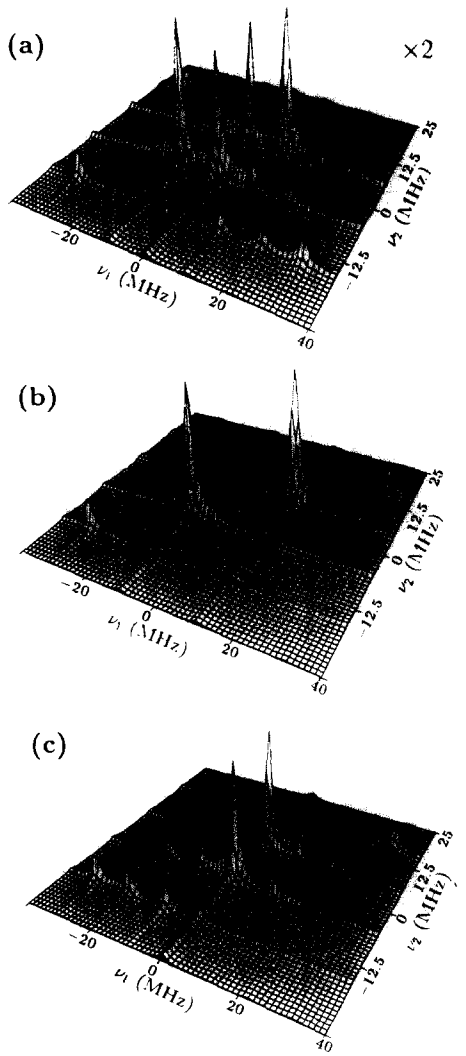

FIG. 2. ESR-SECSY spectra, obtained with (a) S_R, (b) S_{C+}, and (c) S_{C-} for the same case as in Fig. 1, except that here $t_2^{(0)} = 0$ and $\Delta t_1 = 12.5$ (ns). Notice the doubling of frequencies in the ω_1 domain due to our definition of t_1.

function of ω_1. The spectrum of a spin-echo experiment without phase cycling has both the A_1 and the A_3 parts, so it should be compared to the S_R spectrum. If, however, the A_3 term is selected in the spin-echo experiment by the method explained here, this would remove all the "allowed" peaks, which belong to A_1, leaving only the "forbidden" peaks in addition to the central peak, which comes from the "auto-peaks" of A_3. This would make it easier to ascertain whether nuclear modulation is present, even without going to two dimensions.

In a polycrystalline sample, most of the cross peaks are averaged out by the inhomogeneous broadening, as can be seen in Fig. 3, obtained by averaging over 180

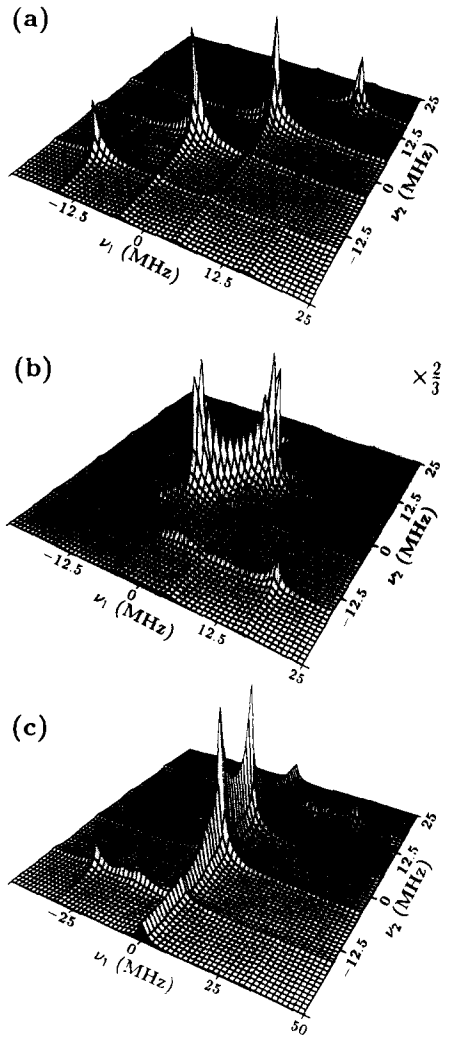

FIG. 3. (a) S_{C+} and (b) S_{C-} ESR-COSY spectra, and (c) S_{C-} ESR-SECSY spectrum of a polycrystalline sample of the same molecules as in Fig. 1. In (c), $t_2^{(0)} = 0$ and $\Delta t_1 = 10$ ns.

orientations of the hyperfine tensor with respect to the magnetic field. Nevertheless, some structure remains, which is helpful in studying the effect of nuclear modulation. Note that only A_3 changes significantly with orientation, so it is this component of the spectrum that is interesting both in 1D and in 2D experiments. The sharpness of the lines on the diagonal results from the long T_2 assumed in the calculation. The structure is smoother, and the cross peaks are somewhat stronger, in the ESR-SECSY spectrum for this case (Fig. 3c). If several nuclei interact with the electron, the relative orientation of their hyperfine tensors gives rise to a spectral structure, most of which is averaged out in a polycrystalline sample (the results of these calculations are not shown here), but in a single crystal the structure is very informative.

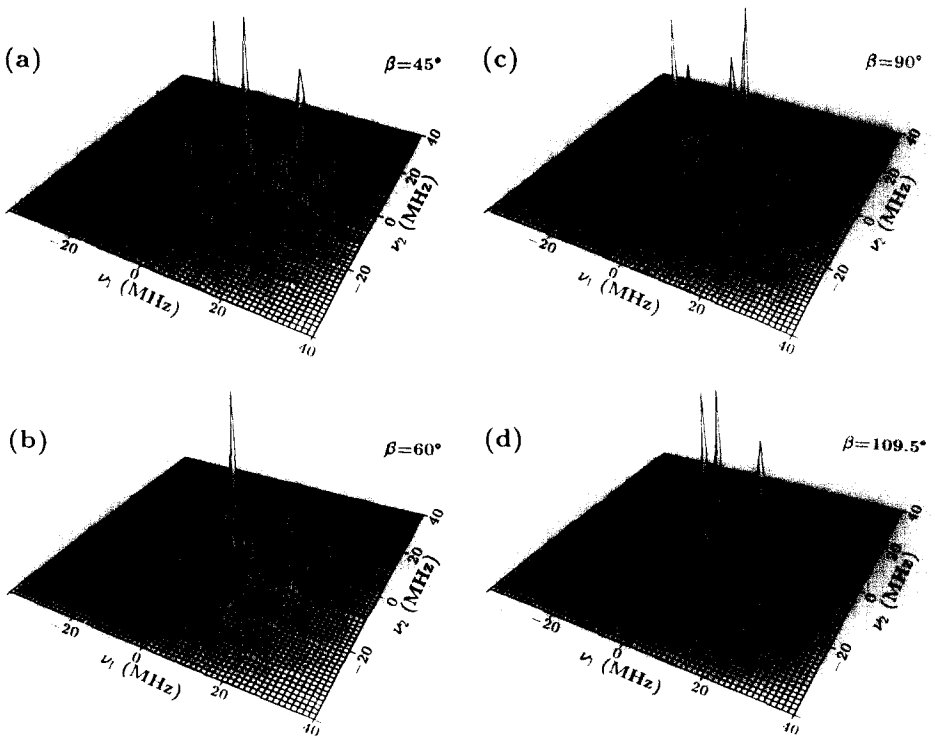

FIG. 4. S_{C-} ESR-COSY spectra for a single crystal with two protons coupled to the electron (parameters as in Fig. 3, except that $\Delta t_1 = \Delta t_2 = 12.5$ ns). The electron-nucleus vector for one proton makes an angle of 30° with the magnetic field, and for the other proton, 30° + β, where β is indicated in the figure. (a) β = 45°, (b) β = 60°, (c) β = 90°, (d) β = 109.5°.

In Fig. 4 the ESR-COSY spectra, in which S_{C-} is selected, are presented for a single crystal with two protons coupled to the electron, with four different relative orientations of the two hyperfine tensors. The detailed lineshapes are sufficiently different to allow an unambiguous determination of the relative angle. The same is true for the corresponding ESR-SECSY spectra, in Fig. 5. But the simulated (Fourier transformed) ESEEM spectra for the same cases, shown in Fig. 6, are not sufficiently detailed for such a clear determination. The S_{C-} ESEEM spectra (with no phase cycling) were computed here, in order to have a proper comparison with Figs. 4 and 5.

When a large number of nuclei interact with the electron, the lineshape is of course more complicated. In Fig. 7 simulated ESR-SECSY lineshapes are presented for a polycrystalline sample of a hypothetical molecule with one nitrogen nucleus, assumed here to be ^{14}N, and 12 protons. These are the same nuclei as in the nitroxide Tempone, but the hyperfine interactions of the protons are assumed to be much stronger than in Tempone (the same as in the previous figures), to show the cumulative effects of strong hyperfine interactions of many protons. The nitrogen hyperfine parameters were taken to be $A_\parallel$ = 32 G, $A_\perp$ = 6 G, and the value of the quadrupole constant is chosen as $D_Q = -1.8$ MHz, corresponding to the value found by Dinse *et*

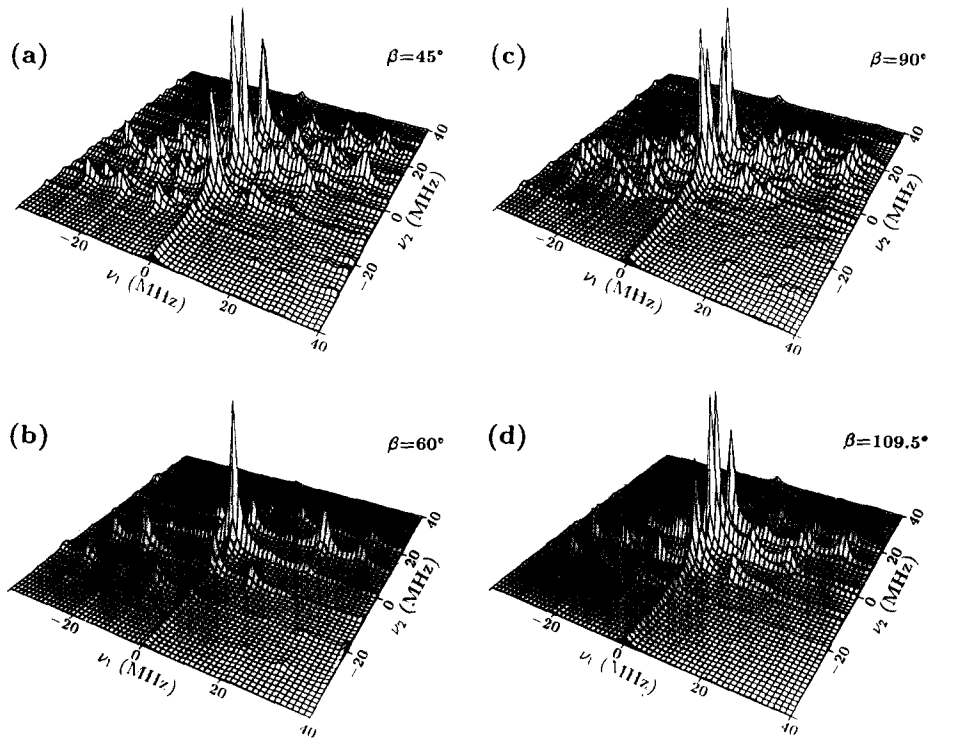

FIG. 5. S_{C-} ESR-SECSY spectra for the same cases as in Fig. 4 (with $t_2^{(0)} = 0$). In the ω_1 domain there is a frequency doubling, due to our definition of t_1.

al. (*26*) (note that our definition differs from theirs by a factor of $\frac{3}{4}$). All protons are assumed to have the same hyperfine interaction with the electron, as actually occurs in Tempone. For simplicity the proton hyperfine tensors are all taken to be collinear with that for the nitrogen nucleus. The lineshapes clearly have some features associated with the nuclear modulation due to the protons. The separate presentation of A_1 (using S_{C+}) and of A_3 (using S_{C-}) is evidently very convenient, because A_3 has an interesting structure due to nuclear modulation. Note also that with the spectral range covered in these simulations, there is for A_1 some aliasing in the ω_1 domain, which is the reason for the appearance of peaks in the upper left corner of Fig. 7a. The A_3 spectrum is shown here from two different angles. In Fig. 7b it is shown parallel to the ω_1 axis, to bring out the different modulation patterns as a function of ω_1 for each value of ω_2. Figure 7c is the same two-dimensional lineshape, viewed parallel to the ω_2 axis, showing the equivalent of a CW spectrum along the $\omega_1 = 0$ axis.

The extra resolution one obtains from the ESR-SECSY experiment is due to the fact that it provides the nuclear modulation patterns for each position in the ESR spectrum from a polycrystalline sample. To the extent that each position in the spectrum is (at least partially) associated with a particular orientation, one obtains the equivalent of "single-crystal-type" nuclear modulations along each slice parallel to the ω_1 axis. This is analogous to the ENDOR technique in polycrystalline samples,

where one can obtain a single-crystal-type NMR spectrum by saturating only a small region of the ESR spectrum, which corresponds to a particular range of orientations (*45*). The advantage of the present method is that all the data are collected at once, with no need to sweep over RF frequencies.

In Fig. 8 similar spectra are presented for "PD-Tempone," with the same assumptions about relative orientations and hyperfine interactions. For the deuterons the hyperfine parameters are chosen as $A_{\parallel} = -0.25$ G, $A_{\perp} = 0.07$ G, and the quadrupole term was neglected. These hyperfine constants are a little more than twice the values expected normally (but they actually yield ESEEM similar to those observed experimentally (*28*)) and are useful for enhancing the effect of nuclear modulation in the present case. In Fig. 8a it is seen that the S_{C+} spectrum is quite sharp, and its shape reflects the nuclear modulation. The S_{C-} spectrum, on the other hand, presented in Fig. 8b, is very broad, which means that for this component of the total lineshape the modulation only causes broadening. Again, viewing this graph from a different angle, one observes a typical nitroxide spectrum along the $\omega_1 = 0$ axis (Fig. 8c). The separation between the S_{C+} and S_{C-} components is therefore very useful for extracting information about the modulation. It should be remembered, however, that in ordinary Tempone the effect of modulation would be weaker, because for $I = 1$ the modulation is stronger than for $I = \frac{1}{2}$ (*2*). An important conclusion from these simulations is that there are, for all practical purposes, no 2D coherence peaks from the ^{14}N nucleus. Only the deuterons or protons in nitroxides are expected to provide any significant coherence peaks. This is also borne out in the study of the three-pulse sequences in the next section.

PHASE CYCLING IN THREE-PULSE SEQUENCES

Theory. The 2D ELDOR pulse sequence is the ESR version of the NMR 2D exchange pulse sequence (*37, 46, 47*). The usefulness of 2D ELDOR was demonstrated in several recent ESR studies, focusing on exchange cross peaks (*18–20, 22*). Our purpose here is to examine how it can be utilized to study nuclear modulation, and also how it can be used to investigate other effects—e.g., exchange effects by suppressing the influence of nuclear modulation when needed. For 2D ELDOR, $\theta_1 = \theta_2 = \theta_3 = \pi/2$ and then the prefactors are (dropping the "(3)" superscript)

$$\alpha_1 = -\frac{i}{8} e^{i\phi_1}, \qquad \alpha_3 = \frac{i}{8} e^{i(2\phi_2 - \phi_1)}$$

$$\alpha_4 = \frac{i}{8} e^{i(\phi_3 - \phi_2 + \phi_1)}, \qquad \alpha_6 = \frac{i}{8} e^{i(\phi_3 + \phi_2 - \phi_1)},$$

$$\alpha_7 = -\frac{i}{8} e^{i(2\phi_3 - 2\phi_2 + \phi_1)}, \qquad \alpha_9 = \frac{i}{8} e^{i(2\phi_3 - \phi_1)}$$

$$\alpha_2 = \frac{i}{4} e^{i\phi_2} = -\beta_1$$

$$\alpha_5 = \beta_2 = 0$$

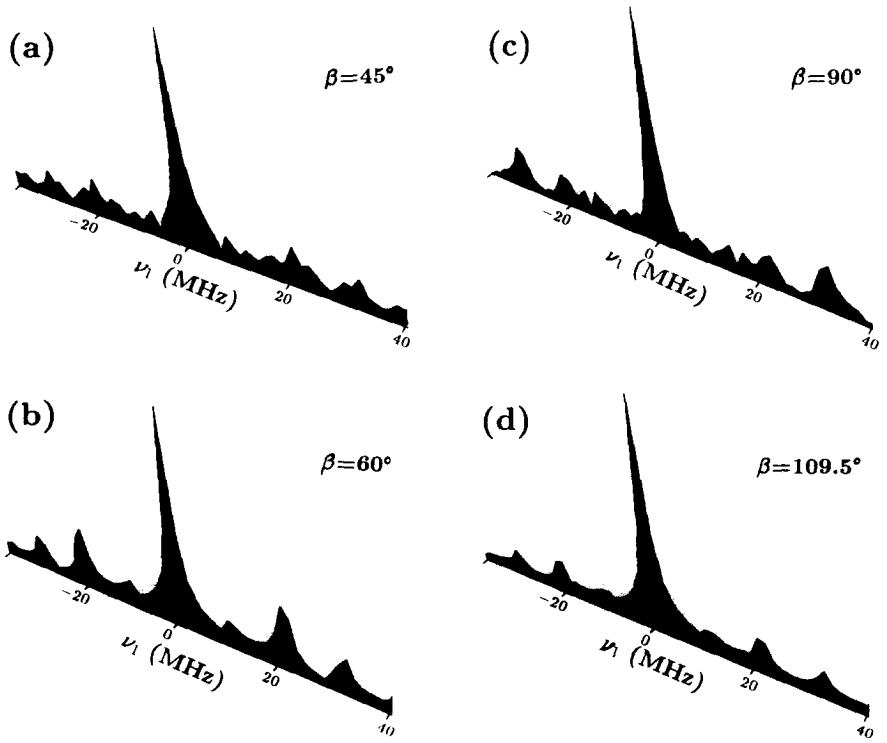

FIG. 6. The Fourier transformed S_{C-} ESEEM spectra for the same cases as in Fig. 4.

$$\alpha_8 = -\frac{i}{4} e^{i(2\phi_3 - \phi_2)} = -\beta_3$$

$$\gamma_1 = -\frac{i}{2} e^{i\phi_3}. \qquad [46]$$

Thus $A_2 + B_1$ and $A_8 + B_3$ are proportional to $(1 - e^{-\tau_1/T_1})$. In the case of no nuclear modulation, i.e., when **M** is the unit matrix, the sum of these four terms reduces exactly to Eq. [35] of Gorcester and Freed for the "axial$_E$" terms (*19*), while C_1 reduces to their Eq. [36] for the "axial$_M$" terms (in this case, $A_5 = B_2 = 0$ if the pulses are exactly $\pi/2$ pulses). For the special case of no nuclear modulation (and no phase cycling), the signal S' is equal to (cf. Eq. [21])

$$S' = \frac{i}{2} e^{-\tau_2/T_1} \sum e^{\lambda_{ji}\tau_3} \mathrm{Re}(e^{\lambda_{ji}\tau_1}) \delta_{i'j'} - \frac{1}{2} \sum e^{\lambda_{ji}\tau_3} \mathrm{Re}(e^{\lambda_{ji}\tau_2}) \mathrm{Im}(e^{\lambda_{ji}\tau_1}) \delta_{i'j'} \qquad [47]$$

and the corresponding S'' signal, obtained by advancing the phase of the first pulse by $\pi/2$, is then

$$S'' = -\frac{i}{2} e^{-\tau_2/T_1} \sum e^{\lambda_{ji}\tau_3} \mathrm{Im}(e^{\lambda_{ji}\tau_1}) \delta_{i'j'} - \frac{1}{2} \sum e^{\lambda_{ji}\tau_3} \mathrm{Re}(e^{\lambda_{ji}\tau_2}) \mathrm{Re}(e^{\lambda_{ji}\tau_1}) \delta_{i'j'}. \qquad [48]$$

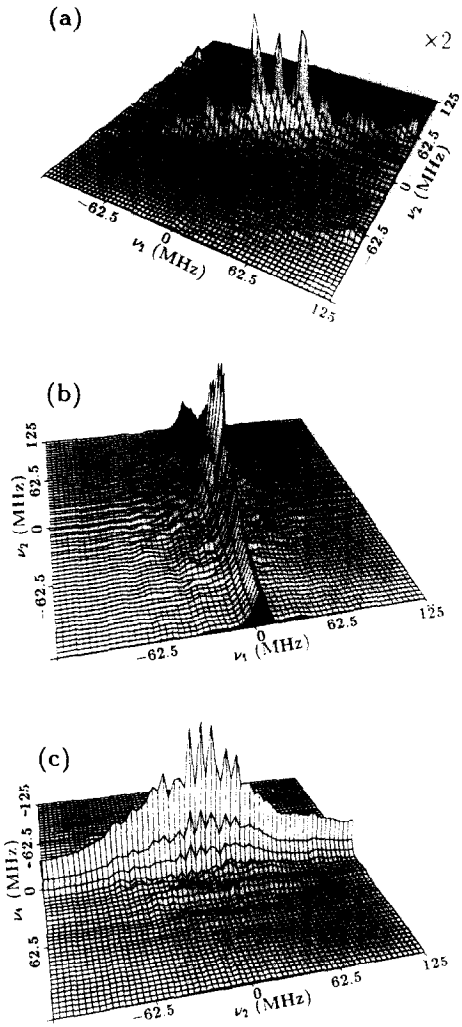

FIG. 7. (a) S_{C+} and (b,c) S_{C-} ESR-SECSY spectra of a polycrystalline sample with an ^{14}N nucleus and 12 ^1H nuclei, all assumed to have hyperfine tensors with the same orientation with respect to the magnetic field. The parameters for the nitrogen nucleus are (in MHz) $\bar{a} = 41.1$, $D = 48.5$, $\nu_I = 1.0$, $F = 14.8$, $D_Q = -1.8$, and for the protons as in Fig. 1. Also, $t_1^{(0)} = 20$, $t_2^{(0)} = 0$, $\Delta t_1 = \Delta t_2 = 4$, and $T_2 = 150$ (all in ns). Note that (b) and (c) show the same 2D spectrum from different viewing directions. The frequency doubling in the ω_1 domain results from our definition of t_1.

In these equations one has to substitute $\tau_1 = t_1$, $\tau_2 = T$ and $\tau_3 = t_2$. These expressions for S' and S'' correspond to the combination of Eqs. [26] and [27] with Eqs. [31] and [32] of Gorcester and Freed (*19*), except for a minor correction (in their Eqs. [31], [32] the factors $\mathrm{Re}(A_n(t_1))$, $\mathrm{Im}(A_n(t_1))$ should be interchanged).

Gorcester and Freed suggested two alternative phase cycles, a 16-step cycle and an 8-step cycle, to cancel the transverse terms (which, in our notation, are A_1, A_7, A_3,

and A_9) and the axial$_E$ terms, which in the present notation are $A_2 + B_1$ and $A_8 + B_3$. On the other hand, in addition to the 2D ELDOR terms (here named A_4 and A_6) their measured signal included also the axial$_M$ (C_1) peaks. As mentioned above, in the general case $A_5 + B_2$ would also be part of the axial$_M$ contribution to the signal. The axial peaks were indirectly eliminated by baseline subtraction. In order to cancel these terms exactly different phase cycles would be necessary.

As in the two-pulse case, using the explicit form of the prefactors (Eq. [46]) and the generalized form taken by each of the prefactors in a phase cycle,

$$\alpha = \kappa \sum_k f_k e^{i(\mu_1 \phi_1^{(k)} + \mu_2 \phi_2^{(k)} + \mu_3 \phi_3^{(k)})}, \qquad [49]$$

it is straightforward to search for a phase cycle which satisfies particular requirements. In Table 4 we present two typical phase cycles that were obtained by a systematic computer search, assuming a given set of receiver factors f_k. In principle the computer search could also include more general choice of receiver factors, but this was not needed for the problem considered here. Both phase cycles cancel exactly all the transverse, axial$_E$ and axial$_M$ terms, and retain the 2D ELDOR terms. In the first of these (Table 4a) steps 1–5 and 9–12 are taken from the 8-step cycle of Gorcester and Freed (converted to our phase convention), which achieves the CYCLOPS image rejection together with the cancellation of the transverse and axial$_E$ parts of the spectrum. The additional steps are required in order to cancel simultaneously also the axial$_M$ part. The other cycle achieves the same selectivity.

As in the two-pulse sequence, S' and S'' may be combined to form S_R, according to Eq. [39] above. Using Eq. [46] we obtain for the individual terms, if all are present,

$$\begin{aligned}
&A_1'' = -iA_1', \quad && A_4'' = -iA_4', \quad && A_7'' = -iA_7' \\
&A_3'' = iA_3', && A_6'' = iA_6', && A_9'' = iA_9' \\
&A_2'' = -A_2', && A_5'' = -A_5', && A_8'' = -A_8' \\
&B_1'' = -B_1', && B_2'' = -B_2' && B_3'' = -B_3', \\
&C_1'' = -C_1'. && && \qquad [50]
\end{aligned}$$

As for the two-pulse sequences, this equation remains valid if some of the individual terms vanish due to phase cycling. Thus, without phase cycling, the S_R combination would not affect the terms A_1, A_4, and A_7, which have peaks on and around the positive diagonal, and would complex conjugate the terms A_3, A_6, and A_9, which are originally on and around the negative diagonal. If the combination S_R is formed, as usual, between the two Fourier transformations, this rotates these latter terms to the positive diagonal. The axial peaks are essentially unaltered. If the Gorcester–Freed phase cycling is applied, only A_4 (on the positive diagonal and around it), A_6 (rotated to the positive diagonal and around it), and $A_5 + B_2 + C_1$ (axial peaks) are present. With the phase cycles in Table 4, only A_4 and A_6 would appear in the spectrum, superimposed one on the other.

If, however, the combination S_{C+} is formed, according to Eq. [41] above, then A_3, A_6, and A_9 are exactly canceled even without any phase cycling, whereas the

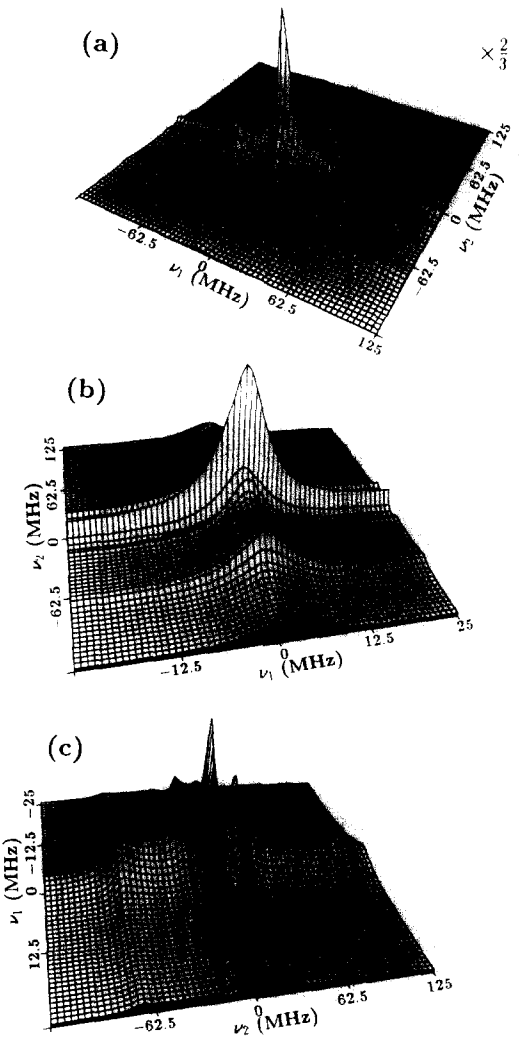

FIG. 8. (a) S_{C+} and (b,c) S_{C-} ESR-SECSY spectra of PD-Tempone. Parameters are as in Fig. 7, except that for the deuterons $\bar{a} = -0.1$, $D = -0.6$, $\nu_I = 2.1$, $F = 0$, and $D_Q = 0$ (all in MHz), and in (b) and (c) $\Delta t_1 = 20$ ns. Note that (b) and (c) refer to different viewing directions of the same 2D spectrum. The frequency doubling in the ω_1 domain is due to our definition of t_1.

combination S_{C-} similarly excludes A_1, A_4, and A_7. Hence in the 2D ELDOR sequence, with the new phase cycles and with one of the two spectral combinations suggested here, only one term—A_4 or A_6—survives the data processing. Thus also for three-pulse sequences the use of quadrature detection enables one to separate the two spectral terms. Although each of these terms contains coherent cross peaks, so that neither of them allows a clean separation of exchange cross-peaks and coherent cross peaks, the spectrum is simplified when A_4 is selected, as explained previously. Finally, if one wants to measure T_1 through the axial$_M$ peaks in the 2D ELDOR experiment,

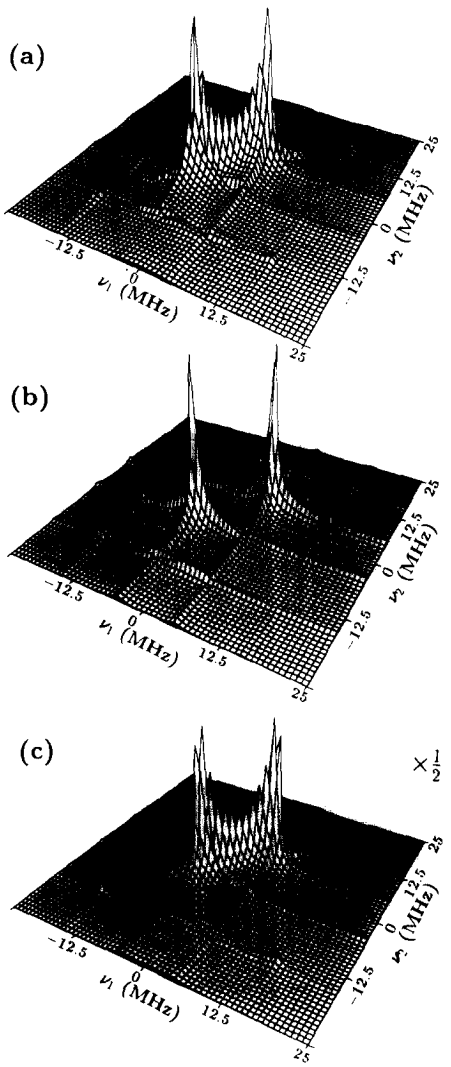

FIG. 9. 2D ELDOR spectra for a polycrystalline sample with one proton (same parameters as in Fig. 3, with the addition of the mixing time $T = 300$ ns).

one has to make all the prefactors, except for α_5, exactly zero. This can be achieved by any of the phase cycles in Table 5.

Results of simulations. A typical 2D ELDOR spectrum, simulated with the S_R spectral combination which selects A_4 and (after rotation) A_6, is shown in Fig. 9a. The sample is taken to be polycrystalline, with just one relevant proton. The corresponding S_{C+} and S_{C-} spectra, showing A_4 and (rotated) A_6 separately, are presented in Figs. 9b and 9c, respectively. These lineshapes clearly resemble very closely the corresponding ESR-COSY lineshapes of Fig. 3, but the existence of a mixing period with the parameter $\tau_2 = T$ does not permit a perfect matching with ESR-COSY. The

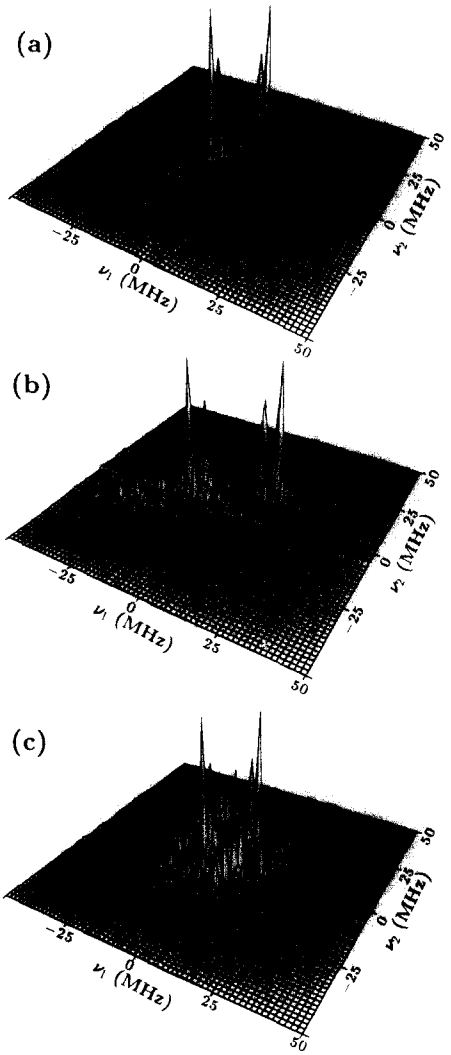

FIG. 10. 2D ELDOR S_{C+} spectra for a single crystal with two protons (same parameters as in Fig. 9. except that $\Delta t_1 = \Delta t_2 = 10$ ns). The symmetry axes of the two hyperfine tensors make angles of 30° and 120° respectively with the magnetic field direction. (a) Ordinary 2D ELDOR. (b) Stimulated echo 2D ELDOR sequence (see text), but this is the "FID term" which continues into the region where the stimulated echo occurs. (c) Refocused 2D ELDOR (see text).

similarity between these two types of spectra may be helpful if it is difficult to distinguish in the 2D ELDOR spectrum between cross peaks resulting from nuclear modulation and those resulting from exchange. The ESR-COSY spectrum for such a system would be related to the "coherent" part of the 2D ELDOR spectrum, and this would help to identify the exchange part.

Figure 10a is the result of a similar computation for a single crystal in which two protons, at different orientations, are coupled to the electron. The S_{C+} combination

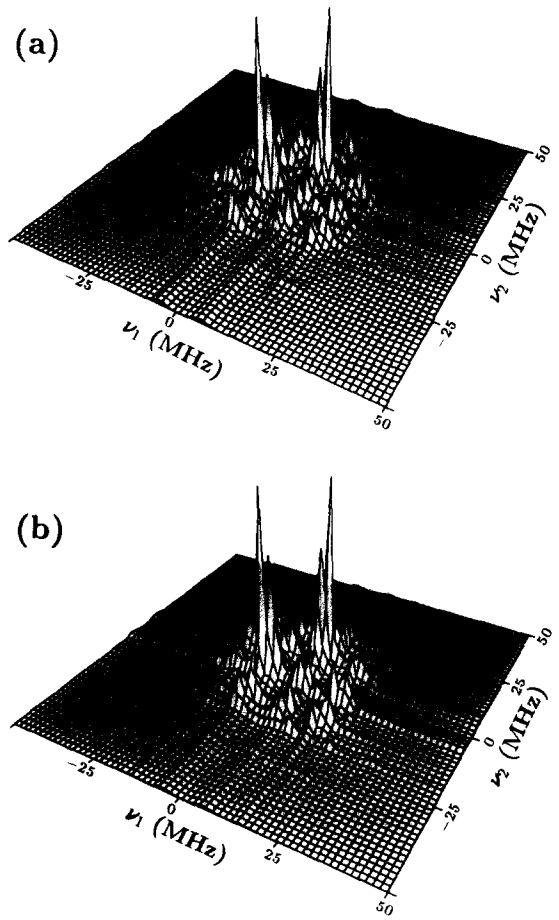

FIG. 11. 2D ELDOR S_{C-} spectra for the same case as in Fig. 10. (a) Ordinary 2D ELDOR. (b) Refocused 2D ELDOR (see text).

was used here. Figure 10b results from such a computation for the stimulated echo version of 2D ELDOR, which is defined by $\tau_1 = t_1$, $\tau_2 = T$, and $\tau_3 = t_1 + t_2$. This experiment is the 2D analog of the stimulated echo experiment, just as ESR-SECSY is the 2D analog of the ordinary spin-echo method. It is quite similar to Fig. 10a except for the frequency doubling in ν_1. In Fig. 10c we see the result of a similar computation for a four-pulse version of 2D ELDOR. To avoid dead-time problems, a fixed delay time and a refocusing π pulse are added, so that the sequence becomes $(\pi/2, \phi_1)$—t_1—$(\pi/2, \phi_2)$—T—$(\pi/2, \phi_3)$—T'—$(\pi, 0)$—$T' + t_2$. The length of T' is chosen to be similar to a typical instrumental dead-time. The phase of the fourth pulse need not be varied, because a perfect π pulse is assumed. As expected for the S_{C+} spectrum, the four-pulse lineshape is more complicated than the three-pulse lineshape of Fig. 10a. If one chooses to use the S_{C-} combination, however, the four-pulse spectrum is quite similar to the three-pulse spectrum, as can be seen in Fig. 11, which again corresponds to the qualitative explanation given above.

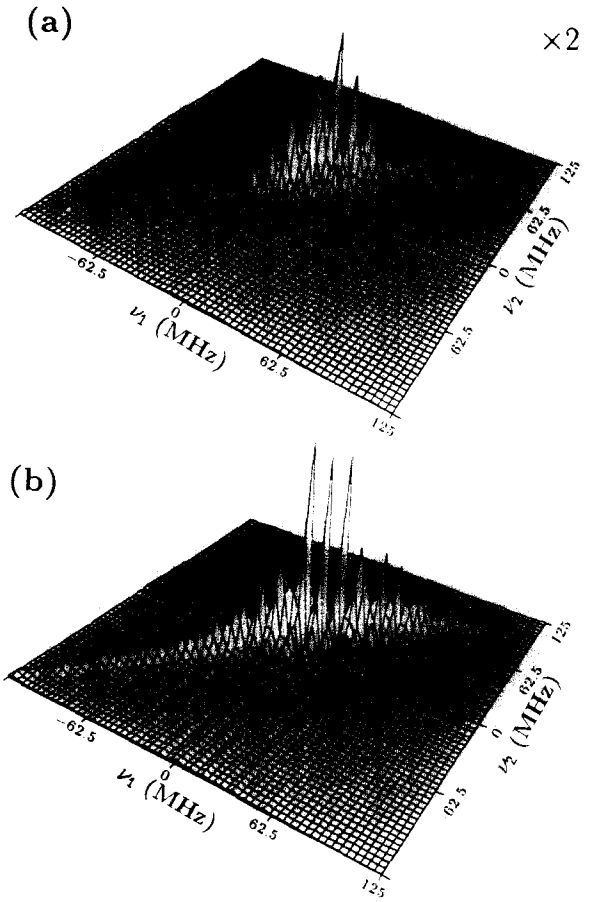

FIG. 12. (a) S_{C+} and (b) S_{C-} 2D ELDOR spectra for the same system as in Fig. 7, with $T = 300$ ns.

In Fig. 12 we show the ordinary 2D ELDOR spectra, simulated with phase cycle 4a and the S_{C+} and S_{C-} spectral combinations, for a system with one nitrogen nucleus and 12 protons, with the same parameters as in the ESR-SECSY simulation of Fig. 7. It is seen that nuclear modulation appears here both in A_4 (Fig. 12a) and in A_6 (Fig. 12b), but it is generally weaker than that which appeared in the ESR-SECSY spectra. The spectra can be smoothed by having a shorter T_2 relaxation time. These spectra show that for 2D ELDOR on such systems one must take into account the effects of nuclear modulation in order to simulate the lineshapes correctly.

The corresponding spectra for PD-Tempone, analogous to the lineshapes in Fig. 8, are shown in Fig. 13. It is clear that in this case the modulation effects are quite small, implying that for nitroxides the 2D ELDOR spectra will not be significantly affected by nuclear modulation.

SUMMARY

A formalism was developed for computing 2D ESR lineshapes that can be obtained with two-pulse or three-pulse sequences, and for some four-pulse sequences, on sys-

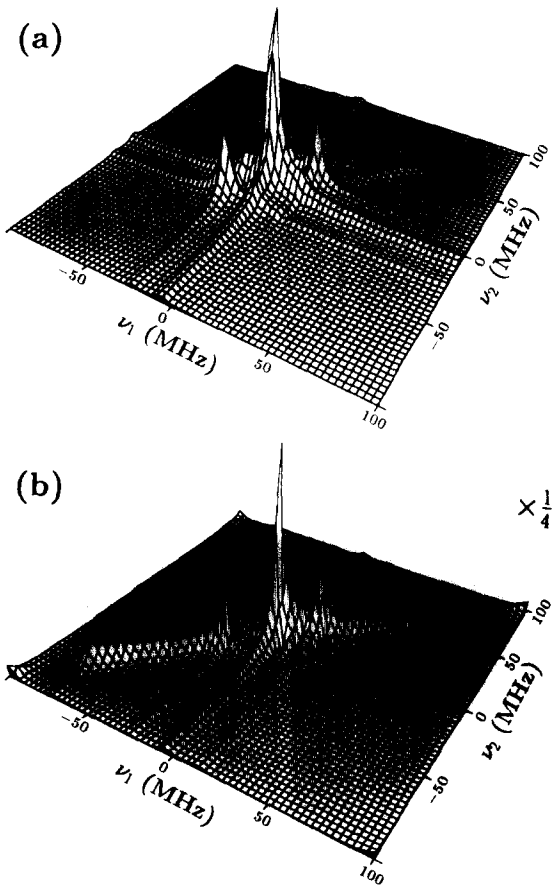

FIG. 13. (a) S_{C+} and (b) S_{C-} 2D ELDOR spectra for PD-Tempone, with the same parameters as in Fig. 8 (except that $\Delta t_1 = \Delta t_2 = 5$ ns), and with $T = 300$ ns.

tems with nuclear modulation. The expressions brought out explicitly the dependence of each component of the spectrum on the Hamiltonian of the observed molecular system on the one hand, and on the durations and phases of the pulses on the other hand. This allowed us to computerize the search for phase cycles which select specific parts of the spectrum. In addition to the phase cycles we showed how to gain further selectivity, when quadrature detection is used, with a simple way of spectral processing, which does not appear to have been used before. A new phase cycle was found, with which one can eliminate in 2D ELDOR all transverse and axial peaks and simultaneously achieve complete image rejection. An analogous phase cycle was found for ESR-COSY, eliminating axial peaks and achieving image rejection. Ways were also found to select in ESR-COSY only the axial term, and in 2D ELDOR only the axial$_M$ terms, for the purpose of measuring T_1. Moreover, it was shown that by combining in 2D ELDOR specific phase cycles with the new way of spectral processing, one could facilitate the distinction between coherent and incoherent cross peaks.

Simulated spectra were shown for various cases, demonstrating the potential of 2D ESR for investigating systems with nuclear modulation. Results were shown for ESR-

COSY, ESR-SECSY, and 2D ELDOR in its ordinary version and in two modified versions, including one with a fourth refocusing pulse. The computed lineshapes for single crystals and for some polycrystalline samples showed that when the spectrum contains structural information, the 2D ESR techniques result in more detailed information, in addition to their capability to probe exchange processes. The simulations also showed for which cases nuclear modulation does not have an appreciable effect on the spectrum, even in the absence of special phase cycling or manipulations of the spectra.

APPENDIX

In this appendix the explicit formulas will be given for the prefactors and the time dependent summations in the various components of the three-pulse ESR signal. The prefactors for Eq. [21] are

$$\alpha_1^{(3)} = -\frac{i}{8} e^{i\phi_1} \sin(\theta_1)(1 + \cos(\theta_2))(1 + \cos(\theta_3))$$

$$\alpha_2^{(3)} = \frac{i}{4} e^{i\phi_2}(1 - \cos(\theta_1))\sin(\theta_2)(1 + \cos(\theta_3))$$

$$\alpha_3^{(3)} = \frac{i}{8} e^{i(2\phi_2 - \phi_1)} \sin(\theta_1)(1 - \cos(\theta_2))(1 + \cos(\theta_3))$$

$$\alpha_4^{(3)} = \frac{i}{8} e^{i(\phi_3 - \phi_2 + \phi_1)} \sin(\theta_1)\sin(\theta_2)\sin(\theta_3)$$

$$\alpha_5^{(3)} = \frac{i}{2} e^{i\phi_3}(1 - \cos(\theta_1))\cos(\theta_2)\sin(\theta_3)$$

$$\alpha_6^{(3)} = \frac{i}{8} e^{i(\phi_3 + \phi_2 - \phi_1)} \sin(\theta_1)\sin(\theta_2)\sin(\theta_3)$$

$$\alpha_7^{(3)} = -\frac{i}{8} e^{i(2\phi_3 - 2\phi_2 + \phi_1)} \sin(\theta_1)(1 - \cos(\theta_2))(1 - \cos(\theta_3))$$

$$\alpha_8^{(3)} = -\frac{i}{4} e^{i(2\phi_3 - \phi_2)}(1 - \cos(\theta_1))\sin(\theta_2)(1 - \cos(\theta_3))$$

$$\alpha_9^{(3)} = \frac{i}{8} e^{i(2\phi_3 - \phi_1)} \sin(\theta_1)(1 + \cos(\theta_2))(1 - \cos(\theta_2))$$

$$\beta_1^{(3)} = -\frac{i}{4} e^{i\phi_2} \sin(\theta_2)(1 + \cos(\theta_3))$$

$$\beta_2^{(3)} = -\frac{i}{2} e^{i\phi_3} \cos(\theta_2)\sin(\theta_3)$$

$$\beta_3^{(3)} = \frac{i}{4} e^{i(2\phi_3 - \phi_2)} \sin(\theta_2)(1 - \cos(\theta_3))$$

$$\gamma_1^{(3)} = -\frac{i}{2} e^{i\phi_3} \sin(\theta_3) \qquad [51]$$

and the corresponding time-dependent factors are

$$
\begin{aligned}
a_1^{(3)} &= \sum e^{\lambda_{ji}\tau_3} e^{\lambda_{ji}\tau_2} e^{\lambda_{ji}\tau_1} |M_{i'j'}|^2 \\
a_2^{(3)} &= e^{-\tau_1/T_1} \sum e^{\lambda_{ji}\tau_3} e^{\lambda_{ji}\tau_2} |M_{i'j'}|^2 \\
a_3^{(3)} &= \sum e^{\lambda_{ji}\tau_3} e^{\lambda_{ji}\tau_2} e^{\lambda_{kl}\tau_1} M_{i'j'} M^\dagger_{j'k'} M_{k'l'} M^\dagger_{l'i'} \\
a_4^{(3)} &= \sum e^{\lambda_{ji}\tau_3} (e^{\lambda_{ji}\tau_2} e^{\lambda_{jk}\tau_1} + e^{\lambda_{ki}\tau_2} e^{\lambda_{li}\tau_1}) M_{i'j'} M^\dagger_{j'k'} M_{k'l'} M^\dagger_{l'i'} \\
a_5^{(3)} &= e^{-\tau_1/T_1} e^{-\tau_2/T_1} \sum e^{\lambda_{ji}\tau_3} |M_{i'j'}|^2 \\
a_6^{(3)} &= \sum e^{\lambda_{ji}\tau_3} (e^{\lambda_{ji}\tau_2} e^{\lambda_{kl}\tau_1} + e^{\lambda_{ki}\tau_2} e^{\lambda_{kl}\tau_1}) M_{i'j'} M^\dagger_{j'k'} M_{k'l'} M^\dagger_{l'i'} \\
a_7^{(3)} &= \sum e^{\lambda_{ji}\tau_3} e^{\lambda_{kl}\tau_2} e^{\lambda_{qp}\tau_1} M_{i'j'} M^\dagger_{j'k'} M_{k'q'} M^\dagger_{q'p'} M_{p'l'} M^\dagger_{l'i'} \\
a_8^{(3)} &= e^{-\tau_1/T_1} \sum e^{\lambda_{ji}\tau_3} e^{\lambda_{kl}\tau_2} M_{i'j'} M^\dagger_{j'k'} M_{k'l'} M^\dagger_{l'i'} \\
a_9^{(3)} &= \sum e^{\lambda_{ji}\tau_3} e^{\lambda_{kl}\tau_2} e^{\lambda_{kl}\tau_1} M_{i'j'} M^\dagger_{j'k'} M_{k'l'} M^\dagger_{l'i'} \\
b_1^{(3)} &= \sum e^{\lambda_{ji}\tau_3} e^{\lambda_{ji}\tau_2} |M_{i'j'}|^2 \\
b_2^{(3)} &= e^{-\tau_2/T_1} \sum e^{\lambda_{ji}\tau_3} |M_{i'j'}|^2 \\
b_3^{(3)} &= \sum e^{\lambda_{ji}\tau_3} e^{\lambda_{kl}\tau_2} M_{i'j'} M^\dagger_{j'k'} M_{k'l'} M^\dagger_{l'i'} \\
c_1^{(3)} &= (1 - e^{-\tau_2/T_1}) \sum e^{\lambda_{ji}\tau_3} |M_{i'j'}|^2.
\end{aligned}
\tag{52}
$$

In these expressions, the states denoted by i, k, p always belong to the subspace in which $S_z = \frac{1}{2}$, and the states denoted by j, l, q belong to the subspace with $S_z = -\frac{1}{2}$. The primes have the same meaning as in Eqs. [17].

For a single proton, it follows from Eqs. [21], [51], and [52] that the S_{C-} signal obtained from the stimulated echo 2D ELDOR (when transversal and axial terms are eliminated by phase cycle 4(a) or 4(b)) contains the decay factor $e^{-(2t_1+t_2)T_2}$ and is proportional to

$$
\begin{aligned}
S = e^{-T/T_1} \Bigg\{ & k_+ \cos(\omega_- t_2) + k_- \cos(\omega_+ t_2) \\
& + \frac{k}{4} \left[\cos\left(\frac{\omega_\alpha}{2}(2t_1 + t_2)\right) \cos\left(\frac{\omega_\beta}{2} t_2\right) + \cos\left(\frac{\omega_\beta}{2}(2t_1 + t_2)\right) \cos\left(\frac{\omega_\alpha}{2} t_2\right) \right] \Bigg\} \\
& + \frac{k}{4} e^{-T/T_2} \left\{ \cos\left(\omega_\alpha(t_1 + T) + \frac{\omega_\alpha}{2} t_2\right) \left[1 - \cos\left(\frac{\omega_\beta}{2}(2t_1 + t_2)\right) \right] \right. \\
& \left. + \cos\left(\omega_\beta(t_1 + T) + \frac{\omega_\beta}{2} t_2\right) \left[1 - \cos\left(\frac{\omega_\alpha}{2}(2t_1 + t_2)\right) \right] \right\}
\end{aligned}
\tag{53}
$$

with the same notation as that in Eq. [45].

ACKNOWLEDGMENTS

The use of the Cornell National Supercomputer Facilities for the computations is gratefully acknowledged. We thank Dr. S. Rananavare for helpful discussions concerning exchange processes.

REFERENCES

1. L. G. ROWAN, E. L. HAHN, AND W. B. MIMS, *Phys. Rev. A* **137,** 61 (1965).
2. W. B. MIMS, *Phys. Rev. B* **5,** 2409 (1972); W. B. MIMS, *Phys. Rev. B* **6,** 3543 (1972).
3. W. B. MIMS, J. PEISACH, AND J. L. DAVIS, *J. Chem. Phys.* **66,** 5536 (1977).
4. G. M. ZHIDOMIROV AND K. M. SALIKHOV, *Theor. Exp. Chem.* **4,** 332 (1968).
5. G. M. ZHIDOMIROV, K. M. SALIKHOV, YU. D. TSVETKOV, V. F. YUDANOV, AND A. M. RAITSIMRING, *J. Struct. Chem.* **9,** 704 (1968).
6. M. K. BOWMAN, L. KEVAN, AND I. M. BROWN, *Chem. Phys. Lett.* **22,** 16 (1973).
7. L. KEVAN, *in* "Time Domain ESR" (L. Kevan and R. N. Schwartz, Eds.), p. 279, Wiley, New York, 1979.
8. S. A. DIKANOV, A. A. SHUBIN, AND V. N. PARMON, *J. Magn. Reson.* **42,** 474 (1981).
9. A. A. SHUBIN AND S. A. DIKANOV, *J. Magn. Reson.* **52,** 1 (1983).
10. M. IWASAKI, K. TORIYAMA, AND K. NUNOME, *J. Chem. Phys.* **86,** 5971 (1986).
11. S. A. DIKANOV AND YU. D. TSVETKOV, *J. Struct. Chem.* **26,** 766 (1985).
12. J. M. FAUTH, A. SCHWEIGER, L. BRAUNSCHWEILER, J. FORRER, AND R. R. ERNST, *J. Magn. Reson.* **66,** 74 (1986).
13. R. P. J. MERKS AND R. DE BEER, *J. Phys. Chem.* **83,** 3319 (1979).
14. P. HÖFER, A. GRUPP, H. NEBENFÜHR, AND M. MEHRING, *Chem. Phys. Lett.* **132,** 279 (1986).
15. G. L. MILLHAUSER AND J. H. FREED, *J. Chem. Phys.* **81,** 37 (1984).
16. G. L. MILLHAUSER AND J. H. FREED, *J. Chem. Phys.* **85,** 63 (1986).
17. L. J. SCHWARTZ, G. L. MILLHAUSER, AND J. H. FREED, *Chem. Phys. Lett.* **127,** 60 (1986).
18. J. GORCESTER AND J. H. FREED, *J. Chem. Phys.* **85,** 5375 (1986).
19. J. GORCESTER AND J. H. FREED, *J. Chem. Phys.* **88,** 4678 (1988).
20. J. GORCESTER AND J. H. FREED, *J. Magn. Reson.* **78,** 292 (1988).
21. G. L. MILLHAUSER, J. GORCESTER, AND J. H. FREED *in* "Electronic Magnetic Resonance of the Solid State" (J. A. Weil, Ed.), p. 571, Canad. Soc. Chemistry, Ottawa, 1987.
22. J. GORCESTER, S. RANANAVARE, AND J. H. FREED, *J. Chem. Phys.* **90,** 5764 (1989).
23. D. J. SCHNEIDER AND J. H. FREED *in* "Advances in Chemical Physics" (J. O. Hirschfelder, R. E. Wyatt, and R. D. Coalson, Eds.), Vol. LXXIII, p. 387, Wiley, New York, 1989.
24. R. R. ERNST, G. BODENHAUSEN, AND A. WOKAUN, "Principles of NMR in One and Two Dimensions," Clarendon Press, Oxford, 1987.
25. J. H. FREED, G. V. BRUNO, AND C. F. POLNASZEK, *J. Phys. Chem.* **75,** 3385 (1971).
26. K. P. DINSE, K. MÖBIUS, M. PLATO, R. BIEHL, AND D. HAUSTEIN, *Chem. Phys. Lett.* **14,** 196 (1972).
27. L. J. SCHWARTZ, A. E. STILLMAN, AND J. H. FREED, *J. Chem. Phys.* **77,** 5410 (1982).
28. L. J. SCHWARTZ, Ph.D. thesis, Cornell University, 1984.
29. G. DROBNY, A. PINES, S. SINTON, D. P. WEITEKAMP, AND D. WEMMER *Faraday Symp. Chem. Soc.* **13,** 49 (1979).
30. D. GAMLIEL, Z. LUZ, AND S. VEGA, *J. Chem. Phys.* **88,** 25 (1988).
31. J. PILÁR, J. LABSKY, J. KÁLAL, AND J. H. FREED, *J. Phys. Chem.* **83,** 1907 (1979).
32. E. MEIROVITCH, D. IGNER, E. IGNER, G. MORO, AND J. H. FREED, *J. Chem. Phys.* **77,** 3915 (1982).
33. E. MEIROVITCH, *J. Phys. Chem.* **88,** 2629 (1984).
34. E. MEIROVITCH, Z. LUZ, AND H. ZIMMERMANN, *J. Phys. Chem.* **88,** 2870 (1984).
35. J. H. FREED, *J. Phys. Chem.* **71,** 38 (1967).
36. M. P. EASTMAN, R. G. KOOSER, M. R. DAS, AND J. H. FREED, *J. Chem. Phys.* **51,** 2690 (1969).
37. S. MACURA, Y. HUANG, D. SUTER, AND R. R. ERNST, *J. Magn. Reson.* **43,** 259 (1981).
38. C. S. JOHNSON, JR., *J. Chem. Phys.* **41,** 3277 (1964).
39. G. BINSCH in "Dynamic NMR Spectroscopy" (L. M. Jackman and F. A. Cotton, Eds.), p. 45, Academic Press, New York, 1975.
40. D. GAMLIEL AND J. H. FREED, *Phys. Rev. A* **39,** 3238 (1989).
41. D. GAMLIEL, Ph.D. thesis, Weizmann Institute of Science, 1988.
42. D. I. HOULT AND R. E. RICHARDS, *Proc. R. Soc. London A* **344,** 311 (1975).
43. P. BACHMANN, W. P. AUE, L. MÜLLER, AND R. R. ERNST, *J. Magn. Reson.* **28,** 29 (1977).
44. D. J. STATES, R. A. HABERKORN, AND D. J. RUBEN, *J. Magn. Reson.* **48,** 286 (1982)
45. G. H. RIST AND J. S. HYDE, *J. Chem. Phys.* **52,** 4633 (1970).
46. J. JEENER, B. H. MEIER, P. BACHMANN, AND R. R. ERNST, *J. Chem. Phys.* **71,** 4546 (1979).
47. S. MACURA AND R. R. ERNST, *Mol. Phys.* **41,** 95 (1980).